Revision 1

Constraints on the origin of sub-effusive nodules from the Sarno (Pomici di Base) eruption of Mt. Somma-Vesuvius (Italy) based on compositions of silicate-melt inclusions and clinopyroxene

Rita Klébesz[1,2,*], Rosario Esposito[1,2], Benedetto De Vivo[2] and Robert J. Bodnar[1]
[1]Department of Geosciences, Virginia Polytechnic Institute and State University, Blacksburg, Virginia 24061, U.S.A.
[2]Dipartimento di Scienze della Terra, dell'Ambiente e delle Risorse, Università di Napoli "Federico II", Naples, 80134, Italy
[*]Present address: MTA CSFK Geodetic and Geophysical Institute, Sopron, 9400, Hungary, e-mail: klebesz.rita@csfk.mta.hu

Abstract

Major and trace element and volatile compositions of reheated melt inclusions (RMI) and their clinopyroxene hosts from a selected "sub-effusive" nodule from the uppermost layer of the Sarno (Pomici di Base; PB) plinian eruption of Mt. Somma-Vesuvius (Italy) have been determined. The Sarno eruption occurred during the first magmatic mega-cycle and is one of the oldest documented eruptions at Mt. Somma-Vesuvius. Based on MI and clinopyroxene composition we constrain processes associated with the origin of the nodule, its formation depth, and hence the depth of the magma chamber associated with the Sarno (PB) eruption. The results contribute to a better understanding of the early stages of evolution of long-lived Mt. Somma-Vesuvius volcanic complex.

The crystallized MI were heated to produce a homogeneous glass phase prior to analysis. MI homogenized between 1202-1256 °C, and three types of RMI were distinguished based on their compositions and behavior during heating. Type I RMI is classified as phono-tephrite – tephri-phonolite – shoshonite, and is the most representative of the melt phase from which the clinopyroxenes crystallized. The second type, referred to as basaltic RMI, have compositions that have been modified by accidentally trapped An-rich feldspar and/or by overheating during homogenization of the MI. The third type, referred to as high-P RMI, is classified as picro-basalt and has high-P content due to accidentally trapped apatite.

Type I RMI are more representative of magmas associated with pre-Sarno eruptions than to magma associated with the Sarno (PB) eruption based on published bulk rock compositions for Mt. Somma-Vesuvius. Therefore, it is suggested that the studied nodule formed from a melt compositionally similar to that which was erupted during the early history of Mt. Somma. The clinopyroxene and clinopyroxene-silicate melt thermobarometer models suggest minimum pressures of 400 MPa (~11 km) for nodule formation, which is greater than pressures and depths commonly reported for the magmas associated with younger plinian eruptions of Mt. Somma-Vesuvius. Minimum pressures of formation based on volatile concentrations of MI interpreted using H_2O-CO_2-silicate melt solubility models indicate formation pressures ≤300 MPa.

Keywords: melt inclusion, homogenization, thermobarometer, Mt. Somma-Vesuvius, nodule, volcanic risk

Introduction

Volcanic activity at Mt. Somma-Vesuvius (Campanian Plain, South Italy) has been the focus of volcanological research for at nearly two millennia, starting with the letters written by Pliny the Younger describing the eruption of Mt. Somma in 79 AD that destroyed Pompeii and killed his uncle, Pliny the Elder. This work has been motivated not only by scientific curiosity but also, in more recent years, by the significant volcanic hazard posed by the proximity of Mt. Somma-Vesuvius to the densely populated city of Naples.

While Mt. Somma – Vesuvius has been active for more than 25 ka, most research has focused on the products of the post-79 AD eruptions. The research focused both on the juvenile products (Ayuso et al. 1998; Barberi et al. 1981; Belkin et al. 1993, 1998; Black et al. 1998; Cioni 2000; Cioni et al. 1995, 1998; Civetta et al. 1991; Fulignati and Marianelli 2007; Joron et al. 1987; Lima et al. 1999; Marianelli et al. 1995, 1999, 2005; Marini et al. 1998; Mastrolorenzo et al. 1993; Mues-Schumacher 1994; Paone 2006, 2008; Piochi et al. 2006a; Raia et al. 2000; Rolandi et al. 1993; Rosi and Santacroce 1983; Santacroce et al. 1993, 2008; Schiano et al. 2004; Somma et al. 2001; Vaggelli et al. 1993; Villemant et al. 1993; Webster et al. 2001) and on the co-genetic or xenolithic lithic fragments, referred to as nodules (Barberi and Leoni 1980; Belkin and De Vivo 1993; Belkin et al. 1985; Cioni et al. 1995; Cundari 1982; Del Moro et al. 2001; Fulignati and Marianelli 2007; Fulignati et al. 1998, 2001, 2004, 2005; Gilg et al. 2001; Hermes and Cornell 1978, 1981; Lima et al. 2003, 2007; Savelli 1968; Sorby 1858). As a result of these studies, the composition of the source region, the structure of the plumbing system, and the pre-eruptive processes and volatile contents of the magmas are fairly well constrained for the post-79 AD eruptions. However, less attention has been devoted to the older eruptions. While abundant data are available for the whole rock compositions of the juvenile products, much less information is available for the melt inclusions (MI).

MI can provide valuable information concerning melt generation and evolution, and the trapping conditions for the MI (Anderson 2003). In addition, MI represent the only tool that can directly provide the pre-eruptive volatile (such as H_2O, CO_2, S, Cl, F) content of a magma. The bulk rock measurements only provide a minimum estimate of volatiles at depth owing to continued degassing during ascent and emplacement on the surface (Lowenstern 2003). In addition, MI from nodules may provide important information related to igneous processes occurring at the magma-country rock interface (e.g., De Vivo et al. 2006).

This study focuses on a sub-effusive nodule (NLM1-1a) previously described by (Klébesz et al. 2012). They reported preliminary results (major and trace element compositions) of MI obtained by analyses of crystallized, unexposed MI using Laser Ablation Inductively-Coupled

Plasma Mass Spectrometry (LA-ICP-MS). This method, however, does not provide information on the volatile content, and the formation *P* and *T* cannot be constrained due to large uncertainties in the major element content associated with analyzing crystallized MI. By heating and homogenizing the MI in the clinopyroxenes, we were able to overcome these obstacles. Major and minor element concentrations of 132 RMI were obtained by Electron Microprobe Analysis (EPMA), trace element concentrations of 73 RMI by LA-ICP-MS, and volatile element concentrations of 32 RMI by Secondary Ion Mass Spectrometry (SIMS). Although homogenization experiments have some disadvantages owing to possible overheating and/or host assimilation, variations related to natural processes and those associated with the heating experiments can often be distinguished. In addition, the obtained data can be used to estimate the formation conditions (*P, T*) of the MI, hence the depth at which the nodule originated or last equilibrated. The results of this study provide constraints that help us to better understand the early stages of evolution of the Mt. Somma-Vesuvius volcanic complex.

Geological background

During the Quaternary period, potassium-rich volcanism developed in central and southern Italy, forming the Roman Co-magmatic Province (Washington 1906) located along the Tyrrhenian margin. The Mt. Somma-Vesuvius volcanic complex is a stratovolcano situated at the southernmost end of the Roman Province, south of the Campanian Plain. The most recent review by De Vivo et al. (2010) summarizes our current knowledge about the source region, plumbing system and volcanic activity of Mt. Somma-Vesuvius, and here we describe the eruptive history briefly.

Eruptive activity associated with the Mt. Somma-Vesuvius volcanic complex started after the highest magnitude eruption in the Campanian Magmatic Province, the Campanian Ignimbrite eruption (39 ka; De Vivo et al. 2001). Other volcanic activity in the area dates back to *ca.* 400 ka (Brocchini et al. 2001; De Vivo et al. 2001; Rolandi et al. 2003; Santacroce et al. 2008 and references therein).

The Mt. Somma-Vesuvius bulk rock compositions define three groups, i.e., three mega-cycles (Arnó et al. 1987; Ayuso et al. 1998; Civetta and Santacroce 1992). In the following, the eruptive history is described according to Rolandi (1997), and in parenthesis the names of eruptions according to Santacroce (1987) are listed. The first mega-cycle lasted from >25 ka to about 14 ka, and includes the older Somma activity, the Codola, the Sarno (Pomici di Base; PB), and the Novelle (Verdoline) plinian eruptions and the subsequent interplinian stages. The second mega-cycle started around 8 ka and lasted until about 2.7 ka, incorporating the Ottaviano (Mercato) and Avellino plinian eruptions and protohistoric interplinian activity. The third mega cycle started in 79 AD with the Pompeii plinian eruption and the subsequent ancient historical interplinian activity. Two other subplinian eruptions belong to this mega-cycle; the 472 AD (Pollena) and the 1631 AD eruptions, both followed by interplinian activity. The last eruption occurred in 1944 and either represents the end of the most recent mega-cycle or simply one of the many eruptions within the continuing third mega-cycle, which would represent an unusually long repose time between eruptions within the continuing third mega-cycle (De Vivo et al. 2010 and references therein).

The products of the first mega-cycle are slightly silica-undersaturated (K-trachyte, K-latite; e.g., Ayuso et al. 1998; Paone 2006; Piochi et al. 2006a; Santacroce et al. 2008). The products of the second mega-cycle are mildly silica-undersaturated (phonotephrites to phonolites; e.g., Ayuso et al. 1998; Piochi et al. 2006a; Santacroce et al. 2008). The third mega-cycle is characterized by strongly silica-undersaturated rocks with tephrite to tephriphonolite-foidite composition (e.g., Ayuso et al. 1998; Piochi et al. 2006a; Santacroce et al. 2008).

Previous studies on nodules from Mt. Somma-Vesuvius

In the Mt. Somma-Vesuvius literature, the term nodule refers to ejecta showing wide variability in composition and texture that are common in the pyroclastic products. Nodules can be metamorphic and/or metasomatized sedimentary rocks, ranging from carbonates to silicic skarn rocks, as well as coarse-grained igneous rocks and cumulate rocks. Zambonini (1910) was the first to describe nodules in the Mt. Somma-Vesuvius deposits, but the classification which has been used recently was proposed by Hermes and Cornell (1978). They divided the Mt. Somma-Vesuvian nodules into four groups: 1) ultramafic cumulates, 2) “skarns”, representing metasomatized carbonates, 3) recrystallized carbonate hornfels, and 4) “sub-effusive” rocks, which are shallow plutonic rocks.

In the Mt. Somma-Vesuvius system, the earlier studies focused on constraining the physical parameters of nodule genesis, but did not consider the geochemical or petrological origin of the nodules or whether they are co-genetic with their pyroclastic hosts. Sorby (1858) studied metasomatized carbonate (skarn) ejecta and concluded that the minerals formed between 340 and 380 °C and at a depth of about 0.6-1 km. Barberi and Leoni (1980) also studied skarns, but they assumed a temperature range of 360-790 °C and a maximum depth of 5-6 km. Cortini et al. (1985) estimated the crystallization temperature of phenocrysts in skarns to be 850-1050 °C, and 1170-1240 °C in cumulates, based on the homogenization temperatures of MI. Belkin and De Vivo (1993) and Belkin et al. (1985) suggested a multistage crystallization history, based on the bimodal distribution of CO_2 fluid inclusion (FI) densities, and estimated 3.5-13 km and 4-10 km for the depth of nodule formation for the interplinian and the plinian eruptions, respectively. Belkin and De Vivo (1993) also noted that FI in nodules from the plinian eruption have higher H_2O-content compared to those from the inter-plinian eruption.

The origin and genesis of the nodules from Mt. Somma-Vesuvius has been controversial. Based on the mineral assemblages and the interstitial glass compositions, Hermes and Cornell (1981, 1983) inferred that the cumulate nodules formed over a range of depths, with a maximum pressure of 300 MPa (~8 km). But, Varekamp (1983) argued that all nodules were derived from the same, shallow source. Savelli (1968) examined carbonate ejecta and concluded, based on the non-equilibrium assemblages, that there was no direct evidence of wall rock assimilation but rather that metasomatism by volcanic fluids and gases was responsible for the observed compositions. Today, it is generally accepted that the silicate crystalline nodules and the skarns represent samples of the heterogeneous wallrock of the magma chamber. The large compositional variations reflect the gradual changes from the carbonate country rock through skarns and metasomatized cumulate rocks to a cumulate crystal mush along the inner walls of the chamber (Cioni et al. 1995). Little information is available about the origin of sub-effusive type nodules that were reported by Hermes and Cornell (1978) from several different eruptions. Most commonly, sub-effusive nodules are interpreted as representing shallow plutonic rocks that usually show compositions equivalent to the erupted lavas or pyroclastics (Belkin and De Vivo 1993; Hermes and Cornell 1978) or intermediate between lava and cumulate compositions (Hermes and Cornell 1978). Hermes and Cornell (1978) suggested that sub-effusive nodules represent the crystal rich part of the crystal mush zone, but this hypothesis was never tested.

Many studies have focused on skarn and silicic nodules from post 79 AD plinian eruptions to understand processes occurring at the magma/wall rock interface and to constrain the underlying plumbing system of the volcano. These studies (Del Moro et al. 2001; Fulignati et al. 1998, 2000, 2001, 2004, 2005; Gilg et al. 2001) concluded that skarn generation can be explained by carbonate wall rock assimilation by mafic alkaline magma that leads to the exsolution of CO_2-rich vapor and complex saline melts from the contaminated magma. These fluids react with the carbonate wall rock resulting in skarn formation. All of the above studies estimate a high (magmatic) temperature, above 700 °C, for skarn formation.

Lima et al. (2003, 2007) constrain the post 79 AD evolution of Mt. Somma-Vesuvius based on compositional data from FI and MI trapped in crystals of nodules. According to their model, separate small magma chambers exist at depths of >3.5 km and possibly a larger chamber is present at a depth of >12 km. In this model, interplinian periods represent a steady state condition under the volcano. During these periods, the volcano acts like an “open system”, indicating that the input of a new supply of magma is always followed by eruption. However, at the end of these periods, cooling of the magma leads to the precipitation of newly formed crystals, which subsequently leads to self-sealing, and hence “closing” of the system. In this situation, the pressure can build up, leading to a subsequent highly explosive plinian eruption. It was also suggested that a carapace forms around the upper portion of the shallow magma chamber (3.6-4.5 km) and acts as an interface between the brittle and plastic rocks (Lima et al. 2007).

Klébesz et al. (2012) studied sub-effusive nodules from the ~20 ka Sarno (PB) eruption. Their study focused mainly on the petrography and mineral chemistry of the nodules. They also reported MI in clinopyroxene. Klébesz et al. (2012) distinguished two types of MI based on petrography, and their classification was supported by compositions determined by LA-ICP-MS. Type I MI contain mica, Fe-Ti-oxide phases and/or dark green spinel, clinopyroxene, feldspar and a vapor bubble. Type II inclusions are generally lighter in color, compared to type I MI, when observed in transmitted light. Generally, Type II MI contain subhedral feldspar, glass, oxides and/or one or more bubbles. Type I MI are classified as phono-tephrite – tephri-phonolite – basaltic trachy-andesite, while Type II MI have basaltic composition (Klébesz et al. 2012). Based on the texture of the nodules and the composition of the minerals and MI, they proposed that the studied nodules originated from crystal-rich mush zones within the plumbing system of Mt. Somma-Vesuvius. In addition, Klébesz et al. (2012) reported that data from crystallized MI suggest magma heterogeneities during the early stages of this volcanic system.

Description of samples and methods

Nodules were collected from the uppermost layer of the Sarno eruption in the Traianello quarry, located on the NE slope of Mt. Somma. The nodules consist of An-rich plagioclase, K-feldspar, clinopyroxene (ferro-diopside), mica (phlogopite-biotite) ± olivine and amphibole and have a porphyrogranular texture. The phenocrysts are large (up to few mm) and show variable compositional zoning. Often irregular intergrowths of alkali feldspar and plagioclase with clinopyroxene, mica and Fe-Ti-oxide minerals are observed. These features are interpreted as crystallized melt pockets. For more detailed information on location of the collected samples, petrographic description and geochemistry of the minerals in the nodule described in this study (NLM1-1a) refer to Type A nodules in Klébesz et al. (2012).

Heating experiments on 67 clinopyroxene crystals from sample NLM1-1a were carried out in the Linkam TS1400 XY heating stage. The specifications of the heating stage and the details of a heating experiment are discussed by Esposito et al. (2012). Heating experiments were conducted during five analytical sessions. In every crystal one MI was preselected and observed continuously and photographed at various times (temperatures) during the heating experiment (Deposit Item-01). Heating was continued until the observed inclusion homogenized, then the sample was quenched. Subsequently, the host crystals were individually mounted in epoxy and polished until the reheated melt inclusion (RMI) was exposed (Thomas and Bodnar 2002). The crystals were removed from the epoxy by a hot needle, and then they were cleaned in distilled water and mounted in a one-inch diameter indium probe mount. A 5 nm evaporative gold coating was applied for the Scanning Electron Microscope (SEM) and for EPMA, and a 30 nm thick sputtered gold coating was applied for SIMS to minimize C-contamination (see Esposito et al. 2014).

Reheated MI (RMI) were analyzed for major and minor elements (SiO_2, TiO_2, Al_2O_3, FeO, MnO, MgO, CaO, Na_2O) by EPMA and for trace elements (Sc, V, Cr, Ni, Rb, Sr, Y, Zr, Nb, Ba, La, Ce, Nd, Sm, Eu, Yb) by LA-ICP-MS. Sample preparation and the specifications of the analytical methods are identical to those described in Klébesz et al. (2012).

RMI were analyzed for volatile (H_2O, CO_2, F, Cl, S) abundances using the SIMS 7f GEO ion probe at Virginia Tech. Analyses were performed using $^{133}Cs^+$ as the source, with a current between 1 and 1.6 nA. A 30 µm x 30 µm spot was rastered within the glass for 240 s to clean the surface before analysis. Then, a 15 µm x 15 µm spot within the rastered area was analyzed using 15 accumulations in depth profile mode. Volatile contents were related to the ratio of the isotope (mass) of interest ($^{16}O^1H$, ^{12}C, ^{19}F, ^{32}S or ^{35}Cl) to ^{30}Si. Four natural standard glasses were used to calibrate the SIMS (EN11346D-2, ALV1649-3, GL07D52-5 and ALV1654-3; Helo et al. 2011). The measured element ratios (e.g., $^{12}C/^{30}Si$) were plotted against the known volatile concentration (e.g., CO_2) of the standard glasses to define the calibration curve. In addition, it has to be emphasized that in some cases the volatile concentration (usually F and sometimes Cl) of the sample was too high and saturated the Faraday cup, therefore, the concentrations of those volatile species could not be determined. Calibration curves used in this study are reported by Esposito et al. (2014) in the deposit items for working session October 2011.

The estimated standard deviation (e.s.d.; 1 sigma) of the EPMA is usually below 5%, if the concentration is above 1 wt%. The e.s.d. (3 sigma) of the LA-ICP-MS analysis was calculated based on Longerich et al. (1996). The 1σ errors based on the slope of each calibration line are 5% relative for CO_2, 3% for H_2O and F, 6% for S, and 1% for Cl [see Deposit item AM-14-508, Octeber_2011 working session in Esposito et al. (2014)]. Based on multiple analyses of three standard glasses, the 1σ reproducibility is 5% for H_2O and F, 6% for S, 14% for CO_2, and 24% for Cl in average. Esposito et al. (2014) analyzed groups of MI all trapped at the same time (melt inclusion assemblage) and estimated SIMS uncertainties of ~10-15% for H_2O and Cl and ~10% for F. It is important to note that Esposito et al. (2014) reported that MI within a single melt inclusion assemblage show large variability for CO_2 and S concentrations that is beyond the SIMS analytical error and likely due to heterogeneity within the MI.

Results

Clinopyroxene chemistry

Clinopyroxenes are present as phenocrysts and in the groundmass of the nodule. Clinopyroxene compositions show some variability, but most can be classified as ferroan diopside based on the compositions obtained by EPMA (Table 1 and Table 1 in Deposit Item-02). Complex compositional zoning is not common in this sample, but normal zoning is occasionally observed.

The MgO content of the clinopyroxene shows only moderate variation, and the calculated mg# [Mg/(Mg+Fe^{total})] ranges between 0.72 and 0.82 (Table 1). No strong correlation was observed between MgO and Cr (Fig. 1b), but in general, clinopyroxenes with higher MgO content tend to have higher Cr concentration, showing up to ~1,300 ppm Cr in some crystals. The MgO content correlates negatively with TiO_2 and Al_2O_3 contents (Fig. 1d), and also with most REE and HFSE (e.g., Zr, Nb). The CaO/Al_2O_3 ratio shows good positive correlation with MgO content (Fig. 1c). Some variation in the trace element concentration is observed, but all samples show similar trace element patterns. The trends defined by major and trace elements and trace element patterns of clinopyroxenes are consistent with fractional crystallization.

Melt inclusions in clinopyroxene

MI in clinopyroxene from the NLM1-1a nodule are either randomly distributed in the crystals or occur along a growth zone that defines a MI assemblage (Bodnar and Student 2006) and are interpreted to be primary (Roedder 1979; Sobolev and Kostyuk 1975). The MI are usually 20-30 µm in maximum dimension, but range from about 5 to 60 µm, and have prismatic shape. They are partially to completely crystallized, indicating (relatively) slow cooling (Roedder 1979). We observed two types of MI, similar to those described by Klébesz et al. (2012).

The homogenization temperature (T_h) of MI in clinopyroxene ranges from 1202 to 1256 °C, but most of the MI show T_h between 1220-1250 °C. However, some other (smaller) MI that were not monitored continuously during heating may have homogenized before the larger MI that were monitored continuously and quenched after homogenization. The T_h does not necessarily equal the trapping temperature (T_t) of the MI. Therefore, if the T_h is below the T_t, the MI can be depleted in the host mineral components, instead if the T_h is above the T_t then the MI can be enriched in those components. However, ratios of elements that are incompatible with the host and elements showing similar concentrations in the melt and the host (e.g., TiO_2, SiO_2, La, Ce, Eu, Zr.) should not be affected significantly by quenching the MI at a *Th* different from T_t (Lima et al. 2003).

For crystallized MI that were analyzed by LA-ICP-MS, it was always possible to determine if the analyzed MI belongs to Type I or Type II based on petrography (Klébesz et al. 2012). In this study, usually one or a small number of MI in each crystal were documented and photographed before the heating experiment, and these MI were monitored continuously during heating to homogenization. However, after heating and then further polishing of the sample to expose the target MI, additional MI that could be analyzed but which had not been documented before heating were often observed. Thus, no record was available for the phases and appearance of these MI before heating. Therefore, we were unable to assign some RMI to the classification of Klébesz et al. (2012) using petrographic data, but instead we classify the RMI based on chemical composition (Table 2 and Table 2 in Deposit Item-02). Thus, RMI with total alkali content >5 wt% are classified as *Type I RMI* (Fig. 2), due to the fact that they have compositions similar to Type I MI in Klébesz et al. (2012). Based on the calculated mg# of the clinopyroxene which would be in equilibrium with the RMI and the measured mg# of the host, only Type I RMI are in, or close to, equilibrium with the clinopyroxene host (Putirka 2008).

A large number (25) of RMI had alkali, silica and trace element contents that were lower than Type I RMI. Here, we refer to these RMI as *basaltic RMI*, owing the fact that they are classified as basalts on the total alkali silica diagram (Fig. 2; Le Bas et al. 1986). No petrographic observations before heating are available for most of the basaltic RMI, but a few (5) are similar to those that were classified as Type II by (Klébesz et al. 2012) based on petrography. Basaltic RMI are usually small (≤20 μm) compared to type I RMI.

Some RMI with picro-basaltic composition (Fig. 2) and with high P_2O_5 (up to 8 wt%) coupled with high CaO/Na_2O ratio (up to 7) were also observed, referred to here as *high-P RMI*. Similar to the basaltic RMI, pre-heating petrographic information was available only for a few high-P RMI. Those high-P RMI are similar to MI that were classified as Type II (Klébesz et al. 2012) based on petrography. Some of the high-P RMI did not homogenize completely, in some cases a small solid phase, that was not large enough to be analyzed, was observed after quenching. This solid phase fluoresced under the focused electron beam. These characteristics suggest that the inclusions trapped silicate melt plus apatite. We have corrected the high-P RMI compositions by subtracting the apatite contribution (using the stoichiometric formula $Ca_5[PO_4]_3OH$) and assuming that the melt contained 0.8 wt% P_2O_5, which is the average P content of Type I RMI, and any P in excess of this value is from trapped apatite. The corrected compositions of the high-P RMI become similar to other RMI.

RMI that are petrographically similar to Type II MI reported by Klébesz et al. (2012) were heated to ~1250 °C during homogenization experiments. These MI appear to homogenize to a silicate melt during heating; however, after quenching and exposing them on the surface of the crystals, these MI were analyzed using the SEM and classified as not having homogenized. A tabular mineral phase surrounded by melt was observed. Some of these mineral phases show plagioclase composition based on EPMA. Sometimes the analyzed phases were smaller than the analytical volume (area) of the EPMA, therefore some of the surrounding material was included in the analysis, resulting in elevated MgO, FeO and lower Al_2O_3 content. We interpret these results as an indication that the MI trapped a plagioclase crystal along with melt and we will refer hereafter to these MI as *Feldspar (Fsp), or fsp-bearing RMI* (Fig. 2).

RMI data show considerable scatter, but general trends are recognizable in the case of Type I RMI when plotted on MgO *vs.* major oxide and trace element variation diagrams (selected diagrams are shown in Fig. 3a-c). The data show an increase in SiO_2, Al_2O_3, K_2O and also in P_2O_5 and Na_2O, and a decrease in CaO and FeO, with decreasing MgO, but no trend in MgO *vs.* TiO_2. Most of the RMI trace elements (Rb, Sr, Zr, Nb, Ba, La, Ce) show increasing abundance with decreasing MgO content for Type I RMI, except for Cr, Sc and Mn. Some of the trace element data show significant scatter and no trend is recognized for MgO *vs.* Y, Nd, Sm, Eu and Yb. Compositions of the RMI of this study and the crystallized MI by Klébesz et al. (2012) partially overlap. However, RMI of this study show a wider compositional range. The observed trends in RMI are consistent with compositional variations resulting from overheating of the MI and incorporation of variable amounts of the host phase into the melt.

In this study, basaltic RMI define a continuous trend from Type I RMI compositions towards more primitive compositions and towards the composition of the host clinopyroxene. It is noteworthy that compositions of basaltic RMI always plot in between the compositions of the Type I RMI, plagioclase and the host clinopyroxene (Fig. 3). This trend is more evident on the Ba/Sr *vs.* 1000/Sr diagram (Fig. 3d), where mixing between end-members defines straight lines. Therefore, the compositions of the basaltic RMI can be derived from the mixing of plagioclase ± Type I melt ± host clinopyroxene.

Volatiles, including F, Cl, S, H_2O and CO_2, were analyzed in selected homogenized MI. The H_2O content was uniformly low, below 0.15 wt%. The CO_2 content varied between 131-1,893 ppm but was mostly below 400 ppm. The F content ranged up to 4,000 ppm but in some cases it is higher because the analytical conditions prevented us from determining the exact concentration because the detector became saturated. The S and Cl contents also vary greatly, reaching maximum concentrations of 156 ppm and 2,771 ppm, respectively. On one hand, no correlation is observed between the volatile abundances when all types of RMI studied (basaltic-RMI, Fsp-MI, High-P, and Type I) are considered, with the exception of S concentration which shows a positive correlation with Cl concentration. On the other hand, we observe some correlations between volatile concentrations and major and trace elements and Mg# of the clinopyroxene host. For example, in Type-1 RMI, Cl increases with increasing S and H_2O. Fluorine shows behavior similar to Cl with the exception of one outlier. Also, S and Cl decrease with increasing Sc, and H_2O shows a strong positive correlation with MnO. Finally, there is a general positive correlation between F, Cl, S, H_2O and the Mg# of the clinopyroxene host and the quenching temperature (Tq).

Considering felspar RMI, basaltic RMI, and High-P RMI, MI show Cl vs. Zr, Rb and La trends toward the origin of the axes with few outliers. Fluorine and Sbehave in a manner similar to Cl. The anomalous RMI show consistent H_2O content between 0.10 and 0.20 wt% with the exception of one High-P RMI that contains 0.05 wt% H_2O.

Discussion

Comparison of the MI data with previously-published results

It was previously suggested by Klébesz et al. (2012) that MI hosted in clinopyroxene from the same nodule studied here record small scale heterogeneities within the melt, which is common at the edges of a magma conduit system (Danyushevsky et al. 2004). However, some RMI of this study that are similar to Type II MI reported by Klébesz et al. (2012) did not homogenize to a glass during heating. In addition, the chemical composition of Type II MI reported by Klébesz et al. (2012) and the basaltic RMI of this study show that the compositions of these MI can be derived by mixing various proportions of melt with an An-rich feldspar and the host clinopyroxene. This observation implies that basaltic RMI are overheated MI that became enriched in clinopyroxene component as a result of overheating and/or the MI trapped a feldspar inclusion along with the silicate melt. This interpretation is further supported by the fact that the inclusion compositions are not in equilibrium with their host. In addition, RMI with anomalously high Mg concentrations are usually smaller than 20 µm (Table 2 in Deposit Item-02). In order to minimize H_2O loss during heating, some MI may have been heated too quickly to maintain equilibrium. Therefore, if the small MI are hosted in a mineral containing larger MI that were observed during the heating experiment, then the smaller MI might have homogenized at a temperature that was lower than the temperature from which the crystal was quenched, and this MI would have therefore been overheated. Based on these observations, we conclude that the different MI compositions do not represent small scale heterogeneities, but rather that basaltic RMI, feldspar RMI and high-P RMI and also Type II MI reported by Klébesz et al. (2012) all trapped mineral phase(s) along with silicate melt in various proportions and which, in some cases, were overheated during microthermometry. This interpretation is supported by Cl, S, and F versus trace elements trends. The solid phase was often An-rich feldspar but in some cases apatite was trapped with the melt, implying that clinopyroxene, apatite, An-rich feldspar and melt were coexisting at the time that the MI were trapped. Therefore, it is likely that only Type I RMI are representative of the melt from which the clinopyroxene crystals grew. Consequently, only Type I MI compositions are compared with data from the literature to investigate the origin of the nodules.

Compositions of MI in various host phases from nodules from different eruptions of Mt. Somma-Vesuvius have been compiled from the literature (Fig. 4). Unfortunately, data are only available for nodules from the 79 AD and younger eruptions. MI in syenite nodules and skarns from the 472 AD eruption (Fulignati and Marianelli 2007; Fulignati et al. 2001) have significantly different compositions than any other MI reported in the literature as well as the MI of this study. Fulignati et al. (2001) interpreted nodules from the 472 AD eruption to represent samples that were broken off of the magma chamber-carbonate wall rock interface and transported to the surface during the eruption. In addition to the highly differentiated phonolitic MI, Fulignati et al. (2001) also found complex chloride-carbonate and hydrosaline melt inclusions, as well as unmixed silicate-salt melt inclusions. Compositions of MI in skarns from the 1944 eruption (Fulignati et al. 2004) do not show such extreme compositions as those from the 472 AD eruption, but still differ from the compositions of MI from cumulate nodules. MI from skarns of the 1944 eruption tend to have lower SiO_2 and MgO content, but higher Al_2O_3, MnO, Na_2O and Cl contents. In addition, hypersaline FI are commonly associated with the MI. The clinopyroxene host in skarns has higher Al_2O_3 content, usually above 7 wt%, compared to clinopyroxenes from the juvenile rocks (Fulignati et al. 2004). The clinopyroxene in this study has significantly lower Al_2O_3 content, usually less than 6 wt%, lacks complex hydrosaline and chloride-carbonate inclusions, and the RMI in this study show compositions similar to MI in cumulate nodules rather than those in skarns. Consequently, the nodules studied here are not thought to represent an environment near the carbonate wall rock, contrary what was previously assumed (Klébesz et al. 2012). However, this does not exclude the possibility that these nodules represent samples of the crystal-mush zone near the magma conduit walls.

Klébesz et al. (2012) concluded that the petrographic features of nodules are consistent with a crystal mush origin, but it is unclear whether these nodules represent the same magma that was erupted during the sustained column phase of the Sarno (PB) eruption or if they crystallized from a melt associated with an older eruption, but were ejected later, during the Sarno eruption. In order to answer this question, Type I RMI were compared to bulk rock compositions of juvenile eruptive products of Mt. Somma-Vesuvius (Fig. 5).

Type I RMI show a continuous trend towards higher CaO/Al_2O_3 when plotted against other indicators of magma evolution (Fig. 5a-e). The least magnesian Type I RMI generally fit within the general trend defined by the Mt. Somma-Vesuvius rocks, whereas the Type I RMI with more primitive compositions (up to about 8 wt% MgO) overlap or show a trend similar to recent Vesuvius volcanics. The recent Vesuvian volcanic rocks define compositional groupings at MgO> ~ 4 wt% and CaO/Al_2O_3> ~ 0.6, as has already been recognized by Danyushevsky and Lima (2001) and Marianelli et al. (1999). According to their interpretations, these rocks do not reflect true melt compositions, but rather represent accumulations of clinopyroxene crystals. Hence, these volcanic rocks represent magmas formed by mixing of evolved melts and various amounts of clinopyroxene crystals inherited from the cumulate layers (Danyushevsky and Lima 2001; Marianelli et al. 1999). The similarities between the trends defined by these volcanics and the Type I RMI of this study support the interpretation that the observed compositional trends are caused by incorporating varying proportions of clinopyroxene component into the melt due to MI overheating. However, there are still some important compositional features that cannot be explained by overheating.

As seen on plots for K_2O and MgO vs. CaO/Al_2O_3 (Fig. 5c-d), it is not possible to account for the disagreement in compositions of the least MgO-rich RMI in clinopyroxene compared to the whole rock trend of the Sarno (PB) and younger eruptions of the first mega-cycle by overheating, regardless of the amount of clinopyroxene component added to the MI by overheating. In other words, the compositions of the most representative (least MgO-rich) RMI in this study are more enriched in MgO, K_2O, TiO_2 and P_2O_5 compared to any known compositions of volcanic rocks from the Sarno (PB) eruption or any other eruptions from the first mega-cycle. The same phenomenon can be observed with trace element systematics (Fig. 5e-g). More specifically, the compositions of MI from the nodules are more enriched in Sc, V, Cr and Ni but depleted in Sr, Y, Zr, Ba and Ce compared to the bulk rock compositions of the Sarno (PB) and younger volcanics of the first mega-cycle. In fact, the compositions of the least magnesian RMI of this study are similar to the compositions of lava rocks from the older Somma (pre-Sarno) activity. Danyushevsky and Lima (2001) reported that these pre-Sarno (PB) rocks can be divided into two groups based on composition of MI hosted in clinopyroxene. The first group has a composition similar to rocks of the first and second mega-cycles (low K-group), while the second group shows high KO_2 and SiO_2 and low Na_2O contents (high-K group). In most cases, the least magnesian compositions of MI in this study overlap with the compositions of the low-K group of older Somma rocks. This overlap is best illustrated by the major elements, but most of the trace elements also show similar behavior (Fig. 5). However, the concentration of some of the trace elements (e.g., Y, Sm, Nd, Eu) spans a wide range and geochemical trends are not well defined.

Despite the wide scatter of the trace element concentrations, the host clinopyroxene crystals in the studied nodule are interpreted to have crystallized from a magma associated with the early Somma activity, prior to the Sarno (PB) eruption, and not from the magma that was erupted during the sustained column phase of the Sarno (PB) eruption. This, however, does not necessarily mean that the entire nodule crystallized from the same magma. Clinopyroxene composition is sensitive to changes in the conditions of crystallization, such as P, T or the melt composition. The simultaneous increase in alumina and HFSE and REE with decreasing MgO is characteristic of normal fractional crystallization. In addition to trends consistent with normal fractionation, no zoning was observed, making it unlikely that the clinopyroxenes in the nodule are xenocrysts. Therefore, the compositions of type I RMI are interpreted to represent melts trapped at various stages during the formation of the nodule.

The origins of the skarns and cumulate nodules are well constrained, but little information is available concerning the origin of sub-effusive type nodules (see above). Although the origin of the nodules in this study cannot be determined with certainty, their presence in the Sarno (PB) eruption indicates that the magma erupted during the Sarno (PB) eruption came from the same (or deeper) magma chamber(s) that fed earlier eruptions. The ascending magma accidentally entrained older, possibly already solidified, rock fragments. If the interstitial liquid had not yet solidified, it would have quenched into glass, as is observed in the cumulate nodules (e.g., Hermes and Cornell 1978).

Pressure and temperature of formation of the nodule

One of the goals of this research was to estimate the formation conditions of the nodules, and use this information to constrain the depth of magma chamber(s) during the early history of the Mt. Somma-Vesuvius volcanic system. The volatile content of the melt trapped in MI is pressure dependent; therefore, the volatile concentration can be used to estimate the minimum trapping pressure assuming a volatile-silicate melt solubility model (e.g., Papale et al. 2006). In addition, formation temperatures may also be estimated using clinopyroxene and clinopyroxene-silicate melt thermobarometers.

The model of Papale et al. (2006) requires as input the composition of the melt, including H_2O and CO_2 concentrations, temperature, and oxidation state. The model calculates the pressure at which the melt would be saturated in these volatiles for the input conditions. If the melt were volatile saturated at the time of MI trapping, then the calculated pressure indicates that actual trapping pressure; if the trapped melt was volatile-undersaturated, the calculated pressure represents a minimum trapping pressure. Evidence for volatile saturation was not observed in the samples of the Sarno (PB) eruption (absence of FI coexisting with MI). For the calculation we assumed the average composition of Type I RMI, a temperature of 1250ºC, and oxidation states defined by $FeO = FeO_{tot}*0.8$ (Fig. 6). The MI showing the maximum CO_2 content suggest a pressure ~300 MPa, but most of the Type I RMI show pressures between 50 and 100 MPa. It is important to emphasize again that the pressures calculated represent minimum trapping pressures as we observed no evidence to suggest that the MI trapped volatile-saturated melts..

Compositions of MI and their host clinopyroxenes were used to estimate the formation conditions for the NLM1-1a nodule using the model of Putirka (2008). Putirka (2008) includes the previously published models of Putirka et al. (1996, 2003) as well as newer models. As discussed above, MI may have become enriched in their host clinopyroxene component as a result of overheating. Published models are unable to correct for overheating, and only those MI that had compositions closest to the equilibrium composition with their host were used. According to Putirka (2008), one way to test for equilibrium is to compare the Fe-Mg exchange coefficient $[K_D(\text{Fe-Mg})^{\text{cpx-liq}}]$ calculated from the MI and its host clinopyroxene composition to a constant value of 0.28 ± 0.08 derived from 1,245 experimental observations. Because the exchange coefficient can vary from 0.04-0.68, with a roughly normal distribution (Putirka 2008), 18 MI-host pairs where the Fe-Mg coefficient was lower than 0.40 were used here. Applying the various thermobarometer models to the selected MI-host pairs, the temperature can be constrained with reasonable certainty, but the pressure varies within wide ranges (Table 3). The model of Putirka et al. (1996) predicted a temperature between 1043-1246 °C, with an average value of 1186 °C. This same model predicts pressures of 120-1630 MPa, with an average of 610 MPa, and with 10 out of 18 pairs between 400-800 MPa. The accuracy of the thermobarometer for a single pair is reported to be at least ± 140 MPa and ± 27 °C, and probably ± 100 MPa and ± 15 °C when averaged over multiple pairs (Putirka et al. 1996). The model of Putirka et al. (2003) estimated temperatures of 980 to 1309 °C, with an average of 1152 °C. The estimated pressure ranges from -280 to 1160 MPa, and 11 out of 18 estimates are between 600 and 1000 MPa. The average estimated pressure is 760 MPa, not including the two negative pressures. The standard error of the pressure estimate is 170 MPa, and for temperature the standard error is 33 K (Putirka et al. 2003). Several newer thermobarometers were also developed by Putirka (2008). Most of these require the input of the H_2O content of the liquid (i.e., the H_2O content of the MI). These equations were not used because the H_2O content in most cases was not measured and, when it was, it was very low (≤0.15 wt%) and it is unclear whether it is representative or not. H_2O might have been lost from the MI during the heating experiments or as a result of hydrogen diffusion during the time the MI resided in the magma before eruption (e.g, Danyushevsky et al. 2002; Lloyd et al. 2013; Severs et al. 2007). Considering that the duration of each heating experiment was similar, the positive correlations between H_2O and Tq and Mg# of Type I RMI suggests that H was significant H_2O loss did not occur during heating experiments.

Putirka (2008) also developed a thermobarometer based on clinopyroxene composition only. A large number (212) of clinopyroxene compositions (several analyses from each crystal, obtained by EPMA) were used to constrain the pressure and temperature of formation based on this model. The temperature estimate is in good agreement with the results given by the previously mentioned thermometers. The estimated temperature of the clinopyroxenes from this study varies between 1019-1366 °C, with an average of 1184 °C. The pressure varies widely, from 160 to 2480 MPa. Over half of the estimates fall between 400 and 800 MPa, with an average of 780 MPa. The standard error of estimate for pressure and temperature is ± 310 MPa and ± 58 °C, respectively (Putirka 2008). In summary, model calculations suggest that clinopyroxene likely crystallized at slightly under 1200 °C. Unfortunately, the thermobarometer models that are available do not constrain the formation pressure of the nodule with high precision. Recognizing these limitations, we conclude that the NLM1-1a nodule most likely formed at ≥400 MPa, corresponding to a depth of at least 11 km. This depth is consistent with a minimum depth of formation calculated based on the H_2O-CO_2 contents of RMI, and this depth is not improbable considering our understanding of the plumbing system of Mt. Somma-Vesuvius, as described below.

The magma feeding system beneath Mt. Somma-Vesuvius consists of three main magma storage levels, the two deepest of which are probably long-lived reservoirs (Piochi et al. 2006b). Isotopic, MI and FI data (Belkin and De Vivo 1993; Belkin et al. 1985; Cioni 2000; Fulignati et al. 2004; Lima et al. 2003, 2007; Marianelli et al. 1999; Piochi et al. 2006b) indicate a shallow reservoir at <6 km, which typically hosts the magmas producing the plinian and sub-plinian eruptions (De Vivo et al. 2010). However, Webster et al. (2012) emphasized that significant concentrations of F, Cl and S can greatly influence the solubility of H_2O and CO_2; hence, geobarometers based on these latter two volatile species may not adequately constrain the pressure conditions, and would underestimate the equilibrium pressure. A deeper magma chamber that supplies the interplinian eruptions was detected at about 8-12 km, and the deepest reservoir is located at >15 km (Piochi et al. 2006b). The deep structure of the plumbing system of the volcanic complex is supported by geophysical evidence as well (De Gori et al. 2001; De Natale et al. 2001, 2006; Nunziata and Costanzo 2010; Nunziata et al. 2006). A low velocity layer is recognized at ~15-35 km depth, which has been interpreted as the deep root for the shallow crustal magma chambers (De Gori et al. 2001; De Natale et al. 2001, 2006; Nunziata et al. 2006).

Thermobarometry results suggest that the PB-Sarno (PB) eruption was fed from magma chambers that are deeper than the magma chambers that supposedly supplied the other plinian eruptions (e.g., 79 AD or Avellino). This is in partial agreement with the findings of Landi et al. (1999), who also predicted that a deep magma chamber fed the Sarno (PB) eruption, but from slightly shallower depths of about 9-12 km. Due to the large variations in the estimated pressures, it cannot be stated with certainty whether a deeper reservoir already existed beneath Mt. Somma-Vesuvius prior to the Sarno (PB) eruption, or if the samples came from the same reservoir that fed the main, "plinian phase" (Landi et al. 1999) of the Sarno (PB) eruption.

Implications

Mt. Somma-Vesuvius is located in a densely populated area of southern Italy, with many hundreds of thousands of people living in the "red" zone surrounding the volcano (e.g., Barnes 2011). Even though it is currently in a dormant state, the volcano is well known for its several plinian eruptions, including the infamous 79 AD eruption that destroyed Pompeii and other nearby towns, and a future violent eruption cannot be excluded. Reducing uncertainty associated with risk assessment requires not only continuous monitoring of the system but also a good understanding of the eruption history and the evolution of the plumbing system of the volcanic complex. Results presented here extend our knowledge of the geochemical conditions associated with eruptions at Mt. Somma-Vesuvius to earlier eruptive events that preceded the 79 AD event, and thus contribute to our understanding of the longer-term history of this volcano. Importantly, our results suggest that plinian eruptions may be fed from magma sources that are deeper than is generally assumed and this, in turn, has important implications for interpreting geophysical data from the perspective of predicting future explosive (plinian) eruptions.

Acknowledgements

The authors would like to thank Paola Petrosino for the field work assistance, Esteban Gazel, Claudia Cannatelli, and Annamaria Lima for valuable discussions concerning volcanic processes and Luca Fedele for help with LA-ICP-MS analyses. The research was partially funded by the PhD Program (XXV Cycle, Coordinated by B. De Vivo) “Internal dynamics of volcanic systems and hydrogeological-environmental risks” of the University of Naples Federico II, (Italy), in collaboration with Virginia Tech in the framework of the Memorandum of Understanding (MoU) signed by the two Universities. This material is based, as well, upon work supported in part by the National Science Foundation under Grant no. EAR-1019770 to RJB. Matthew Severs and an anonymous reviewer are acknowledged for their reviews, and Claudia Cannatelli for her helpful editorial handling.

References cited

Anderson , A.T. (2003) An introduction to melt (glass±crystals) inclusions. In I. Samson, A. Anderson, and D. Marshall, Eds., Fluid Inclusions: Analysis and Interpretation. Mineralogical Association of Canada, Short Course, 32, p. 353-364.

Arnó, V., Principe, C., Rosi, M., Santacroce, R., Sbrana, A., and Sheridan, M.F. (1987) Eruptive History. In R. Santacroce, Ed., Somma-Vesuvius. CNR Quaderni Ricerca Scientifica, 114, p. 53-103.

Ayuso, R.A., De Vivo, B., Rolandi, G., Seal, R.R., and Paone, A. (1998) Geochemical and isotopic (Nd-Pb-Sr-O) variations bearing on the genesis of volcanic rocks from Vesuvius, Italy. Journal of Volcanology and Geothermal Research, 82, 53-78.

Barberi, F., and Leoni, L. (1980) Metamorphic carbonate ejecta from Vesuvius plinian eruptions: Evidence of the occurrence of shallow magma chambers. Bulletin Volcanologique, 43, 107-120.

Barberi, F., Bizouard, H., Clocchiatti, R., Metrich, N., Santacroce, R., and Sbrana, A. (1981) The Somma-Vesuvius magma chamber: a petrological and volcanological approach. Bulletin of Volcanology, 44, 295-315.

Barnes, K. (2011) Volcanology: Europe's ticking time bomb. Nature, 473, 140-140.

Belkin, H.E., and De Vivo, B. (1993) Fluid inclusion studies of ejected nodules from plinian eruptions of Mt. Somma-Vesuvius. Journal of Volcanology and Geothermal Research, 58, 89-100.

Belkin, H.E., De Vivo, B., Roedder, E., and Cortini, M. (1985) Fluid inclusion geobarometry from ejected Mt. Somma-Vesuvius nodules. American Mineralogist, 70, 288-303.

Belkin, H.E., Kilburn, C.R.J., and de Vivo, B. (1993) Sampling and major element chemistry of the recent (A.D. 1631-1944) Vesuvius activity. Journal of Volcanology and Geothermal Research, 58, 273-290.

Belkin, H.E., De Vivo, B., Török, K., and Webster, J.D. (1998) Pre-eruptive volatile content, melt-inclusion chemistry, and microthermometry of interplinian Vesuvius lavas (pre-A.D. 1631). Journal of Volcanology and Geothermal Research, 82, 79-95.

Black, S., Macdonald, R., DeVivo, B., Kilburn, C.R.J., and Rolandi, G. (1998) U-series disequilibria in young (A.D. 1944) Vesuvius rocks: Preliminary implications for magma residence times and volatile addition. Journal of Volcanology and Geothermal Research, 82, 97-111.

Bodnar, R.J., and Student, J.J. (2006) Melt inclusion in plutonic rocks: petrography and microthermometry. In J.D. Webster, Ed., Melt inclusions in plutonic rocks, 36, p. 1-25. Mineralogical Association of Canada.

Brocchini, D., Principe, C., Castradori, D., Laurenzi, M.A., and Gorla, L. (2001) Quaternary evolution of the southern sector of the Campanian Plain and early Somma-Vesuvius activity: insights from the Trecase 1 well. Mineralogy and Petrology, 73, 67-91.

Cioni, R. (2000) Volatile content and degassing processes in the AD 79 magma chamber at Vesuvius (Italy). Contributions to Mineralogy and Petrology, 140, 40-54.

Cioni, R., Civetta, L., Marianelli, P., Metrich, N., Santacroce, R., and Sbrana, A. (1995) Compositional Layering and Syn-eruptive Mixing of a Periodically Refilled Shallow Magma Chamber: the AD 79 Plinian Eruption of Vesuvius. Journal of Petrology, 36, 739-776.

Cioni, R., Marianelli, P., and Santacroce, R. (1998) Thermal and compositional evolution of the shallow magma chambers of Vesuvius, evidence from pyroxene phenocrysts and melt inclusions. Journal of Geophysical Research, 103, 18277-18294.

Civetta, L., and Santacroce, R. (1992) Steady stata magma supply in the last 3400 years of Vesuvius activity. Acta Vulcanologica, 2, 147-159.

Civetta, L., Galati, R., and Santacroce, R. (1991) Magma mixing and convective compositional layering within the Vesuvius magma chamber. Bulletin of Volcanology, 53, 287-300.

Cortini, M., Lima, A., and De Vivo, B. (1985) Trapping temperatures of melt inclusions from ejected Vesuvian mafic xenoliths. Journal of Volcanology and Geothermal Research, 26, 167-172.

Cundari, A. (1982) Petrology of clinopyroxenite ejecta from Somma-Vesuvius and their genetic implications. Tschermaks mineralogische und petrographische Mitteilungen, 30, 17-35.

Danyushevsky, L.V., and Lima, A. (2001) Relationship between Campi Flegrei and Mt. Somma volcanism: evidence from melt inclusions in clinopyroxene phenocrysts from volcanic breccia xenoliths. Mineralogy and Petrology, 73, 107-119.

Danyushevsky, L.V., McNeill, A.W., and Sobolev, A.V. (2002) Experimental and petrological studies of melt inclusions in phenocrysts from mantle-derived magmas: an overview of techniques, advantages and complications. Chemical Geology, 183, 5-24.

Danyushevsky, L.V., Leslie, R.A.J., Crawford, A., and Durance, P. (2004) Melt Inclusions in Primitive Olivine Phenocrysts: the Role of Localized Reaction Processes in the Origin of Anomalous Compositions. Journal of Petrology, 45, 2531-2553.

De Gori, P., Cimini, G.B., Chiarabba, C., De Natale, G., Troise, C., and Deschamps, A. (2001) Teleseismic tomography of the Campanian volcanic area and surrounding Apenninic belt. Journal of Volcanology and Geothermal Research, 109, 55-75.

De Natale, G., Troise, C., Pingue, F., De Gori, P., and Chiarabba, C. (2001) Structure and dynamics of the Somma-Vesuvius volcanic complex. Mineralogy and Petrology, 73, 5-22.

De Natale, G., Troise, C., Pingue, F., Mastrolorenzo, G., and Pappalardo, L. (2006) The Somma-Vesuvius volcano (Southern Italy): Structure, dynamics and hazard evaluation. Earth-Science Reviews, 74, 73-111.

De Vivo, B., Rolandi, G., Gans, P.B., Calvert, A., Bohrson, W.A., Spera, F.J., and Belkin, H.E. (2001) New constraints on the pyroclastic eruptive history of the Campanian volcanic Plain (Italy). Mineralogy and Petrology, 73, 47-65.

De Vivo, B., Lima, A., Kamenetsky, V.S., and Danyushevsky, L.V. (2006) Fluid and melt inclusions in the sub-volcanic environments from volcanic systems: Examples from the Neapolitan area and Pontine Islands, Italy. Mineralogical Association of Canada Short Course 36, p. 211-237, Montreal, Quebec.

De Vivo, B., Petrosino, P., Lima, A., Rolandi, G., and Belkin, H. (2010) Research progress in volcanology in the Neapolitan area, southern Italy: a review and some alternative views. Mineralogy and Petrology, 99, 1-28.

Del Moro, A., Fulignati, P., Marianelli, P., and Sbrana, A. (2001) Magma contamination by direct wall rock interaction: constraints from xenoliths from the walls of a carbonate-hosted magma chamber (Vesuvius 1944 eruption). Journal of Volcanology and Geothermal Research, 112, 15-24.

Esposito, R., Klebesz, R., Bartoli, O., Klyukin, Y., Moncada, D., Doherty, A., and Bodnar, R. (2012) Application of the Linkam TS1400XY heating stage to melt inclusion studies. Central European Journal of Geosciences, 4, 208-218.

Esposito, R., Hunter, J., Schiffbauer, J.D., Shimizu, N., and Bodnar, R.J. (2014) An assessment of the reliability of melt inclusions as recorders of the pre-eruptive volatile content of magmas. American Mineralogist, 99, 976–998.

Fulignati, P., and Marianelli, P. (2007) Tracing volatile exsolution within the 472 AD "Pollena" magma chamber of Vesuvius (Italy) from melt inclusion investigation. Journal of Volcanology and Geothermal Research, 161, 289-302.

Fulignati, P., Marianelli, P., and Sbrana, A. (1998) New insights on the thermometamorphic-metasomatic magma chamber shell of the 1944 eruption of Vesuvius. Acta Vulcanologica, 10, 47-54.

Fulignati, P., Marianelli, P., Santacroce, R., and Sbrana, A. (2000) The skarn shell of the 1944 Vesuvius magma chamber. Genesis and P-T-X conditions from melt and fluid inclusion data. European Journal of Mineralogy, 12, 1025-1039.

Fulignati, P., Kamenetsky, V.S., Marianelli, P., Sbrana, A., and Mernagh, T.P. (2001) Melt inclusion record of immiscibility between silicate, hydrosaline, and carbonate melts: Applications to skarn genesis at Mount Vesuvius. Geology, 29, 1043-1046.

Fulignati, P., Marianelli, P., Santacroce, R., and Sbrana, A. (2004) Probing the Vesuvius magma chamber-host rock interface through xenoliths. Geological Magazine, 141, 417-428.

Fulignati, P., Kamenetsky, V.S., Marianelli, P., and Sbrana, A. (2005) Fluid inclusion evidence of second immiscibility within magmatic fluids (79 AD eruption of Mt. Vesuvius). Periodico di Mineralogia, 74, 43-54.

Gilg, H.A., Lima, A., Somma, R., Belkin, H.E., De Vivo, B., and Ayuso, R.A. (2001) Isotope geochemistry and fluid inclusion study of skarns from Vesuvius. Mineralogy and Petrology, 73, 145-176.

Helo, C., Longpre, M.A., Shimizu, N., Clague, D.A., and Stix, J. (2011) Explosive eruptions at mid-ocean ridges driven by CO_2-richmagmas. Nature Geoscience, 4, 260-263.

Hermes, O.D., and Cornell, W.C. (1978) Petrochemical significance of xenolithic nodules associated with potash-rich lavas of Somma-Vesuvius volcano, NSF final technical report, p. 58, University of Rhode Island.

-. (1981) Quenched crystal mush and associated magma compositions as indicated by intercumulus glasses from Mt. Vesuvius, Italy. Journal of Volcanology and Geothermal Research, 9, 133-149.

Hermes, O.D., and Cornell, W.C. (1983) The significance of mafic nodules in the ultra-potassic rocks from central Italy - reply. Journal of Volcanology and Geothermal Research, 16, 166-172.

Joron, J.L., Metrich, N., Rosi, M., Santacroce, R., and Sbrana, A. (1987) Chemistry and Petrography In R. Santacroce, Ed., Somma-Vesuvius. CNR Quad. Ric. Sci. , 114, p. 105-174, Roma.

Klébesz, R., Bodnar, R., De Vivo, B., Török, K., Lima, A., and Petrosino, P. (2012) Composition and origin of nodules from the ≈20 ka Pomici di Base (PB)-Sarno eruption of Mt. Somma-Vesuvius, Italy. Central European Journal of Geosciences, 4, 324-337.

Landi, P., Bertagnini, A., and Rosi, M. (1999) Chemical zoning and crystallization mechanisms in the magma chamber of the Pomici di Base plinian eruption of Somma-Vesuvius (Italy). Contributions to Mineralogy and Petrology, 135, 179-197.

Le Bas, M.J., Le Maitre, R.W., Streckeisen, A., and Zanettin, B. (1986) A chemical classification of volcanic rocks based on the total alkali-silica diagram. Journal of Petrology, 27, 745-750.

Lima, A., Belkin, H.E., and Török, K. (1999) Understanding Vesuvius magmatic processes: evidence from primitive silicate-melt inclusions in medieval scoria clinopyroxenes (Terzigno Formation). Mineralogy and Petrology, 65, 185-206.

Lima, A., Danyushevsky, L.V., De Vivo, B., and Fedele, L. (2003) A model for the evolution of the Mt. Somma-Vesuvius magmatic system based on fluid and melt inclusion investigations. In B. De Vivo and R.J. Bodnar, Eds., Melt Inclusions in Volcanic Systems: Methods, Applications, Problems. Developments in Volcanology, 5, p. 227-249. Elsevier Press, Amsterdam.

Lima, A., De Vivo, B., Fedele, L., Sintoni, F., and Milia, A. (2007) Geochemical variations between the 79 AD and 1944 AD Somma-Vesuvius volcanic products: Constraints on the evolution of the hydrothermal system based on fluid and melt inclusions. Chemical Geology, 237, 401-417.

Lloyd, A., Plank, T., Ruprecht, P., Hauri, E., and Rose, W. (2013) Volatile loss from melt inclusions in pyroclasts of differing sizes. Contributions to Mineralogy and Petrology, 165, 129-153.

Longerich, H.P., Jackson, S.E., and Gunther, D. (1996) Inter-laboratory note. Laser ablation inductively coupled plasma mass spectrometric transient signal data acquisition and analyte concentration calculation. Journal of Analytical Atomic Spectrometry, 11, 899-904.

Lowenstern, J.B. (2003) Melt Inclusions Come of Age: Volatiles, Volcanoes and Sorby's Legacy. In B. De Vivo and R.J. Bodnar, Eds., Melt Iclusions in Volcanic Systems: Methods, Applications, Problems. Development in Volcanology, 5, p. 1-22. Elsevier Press, Amsterdam.

Marianelli, P., Metrich, N., Santacroce, R., and Sbrana, A. (1995) Mafic magma batches at Vesuvius: a glass inclusion approach to the modalities of feeding stratovolcanoes. Contributions to Mineralogy and Petrology, 120, 159-169.

Marianelli, P., Métrich, N., and Sbrana, A. (1999) Shallow and deep reservoirs involved in magma supply of the 1944 eruption of Vesuvius. Bulletin of Volcanology, 61, 48-63.

Marianelli, P., Sbrana, A., Métrich, N., and Cecchetti, A. (2005) The deep feeding system of Vesuvius involved in recent violent strombolian eruptions. Geophysical Research Letters, 32, L02306.

Marini, L., Chiappini, V., Cioni, R., Cortecci, G., Dinelli, E., Principe, C., and Ferrara, G. (1998) Effect of degassing on sulfur contents and $\delta^{34}S$ values in Somma-Vesuvius magmas. Bulletin of Volcanology, 60, 187-194.

Mastrolorenzo, G., Munno, R., and Rolandi, G. (1993) Vesuvius 1906: a case study of paroxymal eruption and its relation to eruption cycles. Journal of Volcanology and Geothermal Research, 58, 217-237.

Mues-Schumacher, U. (1994) Chemical variation of the A.D. 79 pumice deposits of Vesuvius. European Journal of Mineralogy, 6, 387-395.

Nunziata, C., and Costanzo, M. (2010) Low VS crustal zones in the Campanian Plain (Southern Italy). Mineralogy and Petrology, 100, 215-225.

Nunziata, C., Natale, M., Luongo, G., and F. Panza, G. (2006) Magma reservoir at Mt. Vesuvius: Size of the hot, partially molten, crust material detected deeper than 8 km. Earth and Planetary Science Letters, 242, 51-57.

Paone, A. (2006) The geochemical evolution of the Mt. Somma-Vesuvius volcano. Mineralogy and Petrology, 87, 53-80.

Paone, A. (2008) Fractional crystallization models and B–Be–Li systematics at Mt Somma-Vesuvius volcano (Southern Italy). International Journal of Earth Sciences, 97, 635-650.

Papale, P., Moretti, R., and Barbato, D. (2006) The compositional dependence of the saturation surface of $H_2O + CO_2$ fluids in silicate melts. Chemical Geology, 229, 78-95.

Piochi, M., Ayuso, R.A., De Vivo, B., and Somma, R. (2006a) Crustal contamination and crystal entrapment during polybaric magma evolution at Mt. Somma-Vesuvius volcano, Italy: Geochemical and Sr isotope evidence. Lithos, 86, 303-329.

Piochi, M., De Vivo, B., and Ayuso, R.A. (2006b) The magma feeding system of Somma-Vesuvius (Italy) strato-volcano: new inferences from a review of geochemical and Sr, Nd, Pb and O isotope data. In B. De Vivo, Ed., Volcanism in the Campania Plain: Vesuvius, Campi Flegrei and Ignimbrites, p. Chapter 9: 181-202. Elsevier B. V.

Putirka, K. (2008) Thermometers and Barometers for Volcanic Systems. In K. Putirka and F.J. Tepley III, Eds., Minerals, inclusions and volcanic processes, Reviews in Mineralogy & Geochemistry, 69, p. 61-120. Mineralogical Society of America.

Putirka, K., Johnson, M.C., Kinzler, R., and Walker, D. (1996) Thermobarometry of mafic igneous rocks based on clinopyroxene-liquid equilibria, 0-30 kbar. Contributions to Mineralogy and Petrology, 123, 92-108.

Putirka, K.D., Mikaelian, H., Ryerson, F., and Shaw, H. (2003) New clinopyroxene-liquid thermobarometers for mafic, evolved, and volatile-bearing lava compositions, with applications to lavas from Tibet and the Snake River Plain, Idaho. American Mineralogist, 88, 1542-1554.

Raia, F., Webster, J.D., and De Vivo, B. (2000) Pre-eruptive volatile contents of Vesuvius magmas: constraints on eruptive history and behavior. I - The medieval and modern interplinian activities. European Journal of Mineralogy, 12, 179-193.

Roedder, E. (1979) Origin and significance of magmatic inclusions. Bulletin de Mineralogie, 102, 487-510.

Rolandi, G. (1997) The eruptive history of Somma-Vesuvius. In M. Cortini and B. De Vivo, Eds., Volcanism and Archeology in Mediterranean Area. Reserch Signpost, p. 77-88. Trivandrum.

Rolandi, G., Barrella, A.M., and Borrelli, A. (1993) The 1631 eruption of Vesuvius. Journal of Volcanology and Geothermal Research, 58, 183-201.

Rolandi, G., Bellucci, F., Heizler, M.T., Belkin, H.E., and De Vivo, B. (2003) Tectonic controls on the genesis of ignimbrites from the Campanian Volcanic Zone, southern Italy. Mineralogy and Petrology, 79, 3-31.

Rosi, M., and Santacroce, R. (1983) The 472 A.D. 'Pollena' eruption: volcanological and petrological data for this poorly known plinian-type event at Vesuvius. Journal of Volcanology and Geothermal Research, 17, 249-271.

Santacroce, R. (1987) Somma-Vesuvius. CNR Quaderni della Ricerca Scientifica 114, 8, p. 251.

Santacroce, R., Bertagnini, A., Civetta, L., Landi, P., and Sbrana, A. (1993) Eruptive dynamics and petrogenetic processes in a very shallow magma reservoir: The 1906 eruption of Vesuvius. Journal of Petrology, 34, 383-425.

Santacroce, R., Cioni, R., Marianelli, P., Sbrana, A., Sulpizio, R., Zanchetta, G., Donahue, D.J., and Joron, J.L. (2008) Age and whole rock-glass compositions of proximal pyroclastics from the major explosive eruptions of Somma-Vesuvius: A review as a tool for distal tephrostratigraphy. Journal of Volcanology and Geothermal Research, 177, 1-18.

Savelli, C. (1968) The problem of rock assimilation by Somma-Vesuvius magma. Contributions to Mineralogy and Petrology, 18, 43-64.

Schiano, P., Clocchiatti, R., Ottolini, L., and Sbrana, A. (2004) The relationship between potassic, calc-alkaline and Na-alkaline magmatism in South Italy volcanoes: A melt inclusion approach. Earth and Planetary Science Letters, 220, 121-137.

Severs, M.J., Azbej, T., Thomas, J.B., Mandeville, C.W., and Bodnar, R.J. (2007) Experimental determination of H_2O loss from melt inclusions during laboratory heating: Evidence from Raman spectroscopy. Chemical Geology, 237, 358-371.

Sobolev, V.S., and Kostyuk, V.P. (1975) Magmatic crystallization based on a study of melt inclusions. "Nauka" Press (in Russian; translated in part in Fluid Inclusion Research, 9, 182-253), Novosibirsk.

Somma, R., Ayuso, R.A., De Vivo, B., and Rolandi, G. (2001) Major, trace element and isotope geochemistry (Sr-Nd-Pb) of interplinian magmas from Mt. Somma-Vesuvius (Southern Italy). Mineralogy and Petrology, 73, 121-143.

Sorby, H.C. (1858) On the Microscopical, Structure of Crystals, indicating the Origin of Minerals and Rocks. Quarterly Journal of the Geological Society, 14, 453-500,.

Thomas, J.B., and Bodnar, R.J. (2002) A technique for mounting and polishing melt inclusions in small (<1mm) crystals. American Mineralogist, 87, 1505-1508.

Vaggelli, G., De Vivo, B., and Trigila, R. (1993) Silicate-melt inclusions in recent Vesuvius lavas (1631-1944): II. Analytical chemistry. Journal of Volcanology and Geothermal Research, 58, 367-376.

Varekamp, J.C. (1983) The significance of mafic nodules in the ultra-potassic rocks from central Italy - discussion. Journal of Volcanology and Geothermal Research, 16, 161-165.

Villemant, B., Trigila, R., and DeVivo, B. (1993) Geochemistry of Vesuvius volcanics during 1631–1944 period. Journal of Volcanology and Geothermal Research, 58, 291-313.

Washington. (1906) The roman comagmatic Region. 199 p. Carnegie Inst Washington Publ. No. 57.

Webster, J.D., Raia, F., De Vivo, B., and Rolandi, G. (2001) The behavior of chlorine and sulfur during differentiation of the Mt. Somma-Vesuvius magmatic system. Mineralogy and Petrology, 73, 177-200.

Webster, J.D., Goldoff, B., Sintoni, F., and De Vivo, B. (2012) Solubilities of H-O-C-S-Cl volatiles in fluids and silicate melts and their control on magmatic processes. Mineralogical Magazine, 76, 2532.

Zambonini, F. (1910) Mineralogia Vesuviana. Atti delle Reale Accademia delle Scienze Fisiche e Matematiche di Napoli, Ser. 2°, 14, 1-463.

Figure Captions

Figure 1. Variation diagrams of representative major and trace elements in clinopyroxene from nodule NLM1-1a from the Sarno (Pomici di Base) eruption of Mt. Somma-Vesuvius (Italy). a) Spider diagram of clinopyroxene compositions normalized to primitive mantle. Trace element concentrations determined by LA-ICP-MS. b) Cr vs MgO, c) CaO/Al_2O_3 vs. MgO, and d) Al_2O_3 vs, MgO. Error bars in panels b), c), and d) indicate the average standard deviations. Major element concentrations of panels b), c), and d) were determined by EPMA, Cr was determined by LA-ICP-MS.

Figure 2. Composition of MI hosted in clinopyroxene from sample NLM1-1a plotted on the total alkali silica diagram (Le Bas et al. 1986). All data recalculated to 100% anhydrous. Average estimated standard deviation is smaller than the size of the symbols. Data were obtained by EPMA. Grey fields represent MI data from Klébesz et al. (2012).

Figure 3. Composition of MI hosted in clinopyroxene from sample NLM1-1a. a) MgO vs. CaO, b) MgO vs. TiO_2, c) MgO vs. La, d) 1000/Sr vs. Ba/Sr. Dashed lines indicate mixing between end-members. Error bars on panels b) and c) indicate the average standard deviation. All data recalculated to 100% anhydrous. Major and minor element concentrations of panels a), b) and c) were determined by EPMA, trace element concentrations of panel d) by LA-ICP-MS.

Figure 4. Comparisons between the compositions of Type I RMI (this sudy) and compositions of MI in skarn and cumulate nodules from the literature (Fulignati and Marianelli 2007; Fulignati et al. 2001, 2004; Hermes and Cornell 1981; Lima et al. 2003, 2007). a) CaO/Al_2O_3 vs. MnO, b) CaO/Al_2O_3 vs. MgO, c) CaO/Al_2O_3 vs. SiO_2. Error bars indicate the average standard deviation. All data recalculated to 100 % anhydrous. MI data representative of skarn and cumulate nodules from Mt. Somma-Vesuvius are shown by grey fields. Data of this study were obtained by EPMA.

Figure 5. Comparison of compositions of Type I RMI in clinopyroxene from sample NLM1-1a with bulk rock compositions of juvenile eruptive rocks from Mt. Somma-Vesuvius. a) CaO/Al_2O_3 vs. SiO_2, b) CaO/Al_2O_3 vs. Na_2O, c) CaO/Al_2O_3 vs. K_2O, d) CaO/Al_2O_3 vs. MgO, e) CaO/Al_2O_3 vs. Ba, f) and g) K_2O/Ba vs. Sr/Zr. Bulk rock data, indicated by grey fields, are from the literature (see text). All data recalculated to 100% anhydrous. Average estimated standard deviations are smaller than the size of the symbols. On panel g) full, dashed and dotted lines indicate the compositional trend of the bulk rocks of the third, second and first mega-cycles, respectively. Major and minor element concentrations were determined by EPMA, trace element concentrations by LA-ICP-MS.

Figure 6. H_2O-CO_2 systematics of RMI from this study. The isobars were calculated using the H_2O-CO_2-silicate melt solubility model by Papale et al. (2006). For the calculation, we assumed

the average composition of Type I RMI for the melt, a temperature of 1250ºC, and redox conditions controlled by FeO = FeO_{tot}*0.8. Note that the maximum pressure estimated for Type I RMI plots close to the 300 MPa isobar. This pressure is considered a minimum trapping pressure due to the effect of overheating and absence of volatile saturation. Error bars indicate the average standard deviation. Volatile compositions were obtained by SIMS.

Table 1. Representative analyses of clinopyroxene from sample NLM1-1a

Sample:	**cpx165**	**cpx153**	**cpx151**	**cpx143 (B)**	**cpx143 (C)**	**cpx140**	**cpx110**	**cpx05**	**cpx117**	**cpx116**	**cpx159**	**cpx139**	**cpx150**
SiO_2	49.98(17)	48.00(17)	50.63(20)	49.46(20)	51.08(20)	49.12(26)	50.89(20)	49.85(20)	49.84(20)	49.81(20)	49.76(17)	50.38(20)	48.28(20)
TiO_2	1.10(3)	1.22(3)	0.93(3)	1.18(3)	0.89(3)	1.51(5)	0.75(2)	0.76(2)	1.10(3)	1.03(3)	1.18(3)	1.33(3)	1.61(4)
Al_2O_3	4.90(5)	5.07(5)	4.63(5)	6.11(6)	3.91(5)	6.37(8)	3.84(4)	4.72(5)	4.47(5)	4.49(5)	4.79(5)	5.45(6)	6.40(6)
FeO	7.61(13)	8.15(13)	6.59(12)	7.03(12)	6.59(12)	8.32(19)	6.66(12)	6.38(11)	7.94(14)	7.92(14)	7.55(13)	7.63(13)	8.11(13)
MnO	0.20(3)	0.15(3)	0.16(3)	0.20(4)	0.17(3)	0.16(5)	0.17(3)	0.12(3)	0.13(3)	0.22(4)	0.20(4)	0.19(3)	0.18(4)
MgO	14.09(10)	13.87(10)	14.53(10)	13.80(9)	14.73(10)	13.18(13)	15.12(11)	14.77(11)	13.99(10)	14.13(10)	13.95(10)	13.86(10)	12.93(9)
CaO	22.05(12)	21.05(12)	21.85(11)	21.65(11)	22.23(11)	21.31(15)	22.40(12)	22.74(12)	22.04(12)	22.08(12)	21.48(12)	21.83(11)	21.70(11)
Na_2O	0.36(2)	0.38(2)	0.32(2)	0.32(2)	0.28(2)	0.44(4)	0.26(2)	0.25(2)	0.33(2)	0.34(2)	0.33(2)	0.35(2)	0.35(2)
Total	100.37	97.97	99.70	100.00	100.12	100.46	100.21	99.79	99.87	100.09	99.26	101.12	99.66
Sc	126(155)	104(160)	109(163)	119(161)	116(163)	125(163)	123(144)	116(132)	126(141)	126(155)	108(164)	117(159)	138(191)
V	461(8)	455(10)	396(11)	373(10)	430(10)	483(10)	449(10)	448(8)	493(8)	353(9)	389(11)	435(9)	507(12)
Cr	699(7)	252(9)	1203(10)	604(9)	456(9)	381(8)	1025(8)	291(7)	190(8)	651(7)	209(9)	541(8)	878(10)
Ni	81(4)	97(4)	93(4)	72(4)	102(4)	100(4)	107(4)	86(4)	82(4)	85(5)	86(4)	94(4)	77(4)
Rb	-	-	-	-	-	-	-	-	-	1.7(28.1)	-	-	-
Sr	92(2)	92(2)	84(2)	83(3)	93(3)	93(2)	88(2)	110(2)	94(2)	83(3)	85(3)	89(3)	90(3)
Y	28.5(2.7)	34.8(2.8)	18.8(2.9)	27.3(3.8)	23.0(3.8)	40.4(2.9)	24.9(2.5)	36.9(2.0)	41.3(2.3)	29.6(3.5)	29.0(3.5)	30.0(2.8)	34.3(2.8)
Zr	91(2)	93(2)	52(2)	79(2)	62(2)	138(2)	70(3)	101(1)	120(2)	83(1)	80(2)	85(1)	120(1)
Nb	0.4(4.5)	0.5(4.9)	-	0.4(5.4)	0.2(5.4)	0.5(5.0)	0.3(4.0)	0.6(3.4)	0.5(3.8)	0.6(3.8)	0.4(4.6)	0.4(4.8)	0.5(5.7)
Ba	0.4(2.0)	1.0(2.0)	0.2(1.4)	4.7(1.5)	0.2(1.5)	0.6(1.6)	0.5(1.5)	8.9(1.4)	0.4(1.6)	1.0(1.6)	0.2(2.4)	0.3(1.9)	0.4(1.6)
La	8.7(1.2)	8.7(2.5)	5.4(3.1)	7.3(2.4)	6.6(2.4)	11.3(1.8)	6.9(1.9)	13.5(1.1)	11.5(1.7)	7.6(2.9)	7.8(1.8)	8.4(2.5)	10.4(2.1)
Ce	30.6(0.8)	33.1(1.6)	20.9(1.9)	26.7(1.9)	21.9(1.9)	37.8(1.3)	23.8(1.2)	42.4(1.0)	39.1(1.1)	26.0(1.3)	28.5(1.5)	30.9(1.6)	37.5(2.4)
Nd	30.7(2.5)	32.7(2.4)	20.9(2.5)	27.2(2.8)	22.3(2.8)	40.7(2.7)	23.8(2.4)	40.4(1.7)	41.1(1.7)	28.2(2.8)	27.9(2.1)	31.4(2.9)	37.9(2.9)
Sm	9.5(1.5)	10.0(1.9)	5.8(1.6)	8.7(2.3)	6.8(2.3)	11.7(2.0)	7.5(1.1)	11.9(1.2)	12.0(0.9)	8.8(1.4)	9.0(1.1)	10.0(1.9)	10.4(1.6)
Eu	2.0(1.4)	2.2(1.3)	1.2(1.9)	2.0(2.2)	1.7(2.3)	2.7(1.8)	1.8(2.1)	2.6(1.4)	2.9(1.9)	1.8(1.9)	2.1(1.3)	2.1(2.1)	2.5(2.3)
Yb	2.2(1.2)	2.7(1.7)	1.4(1.6)	2.2(1.8)	1.4(1.9)	3.0(1.6)	2.0(0.9)	3.1(1.0)	3.4(1.2)	2.6(1.4)	1.9(1.9)	2.9(1.0)	2.9(1.2)
mg#	0.82	0.83	0.82	0.80	0.82	0.77	0.86	0.88	0.81	0.83	0.79	0.78	0.78
En	41	41	43	41	43	40	43	42	41	41	41	41	39
Wo	46	45	46	47	46	46	46	47	46	46	46	46	47
Fs	13	14	11	12	11	14	11	10	13	13	13	13	14

mg# = $Mg/(Mg+Fe^{2+})$; En, Wo, Fs, enstatite, wollastonite, ferrosilite in mol% of clinopyroxene; -, below detection limit; major and minor elements are in wt%, trace elements are in ppm. Major and minor elements were determined by EPMA, trace elements by LA-ICP-MS. Estimated standard deviation (e.s.d.) is indicated in parentheses.

Table 2. Composition of representative RMI in clinopyroxene

	Fsp or fsp-bearing MI			Basaltic RMI						High-P RMI		
Sample	**cpx134p2_A**	**cpx157_A**	Sample	**cpx05_A2**	**cpx901_A**	**cpx116_B**	**cpx05_C**	**cpx123p1_B**	Sample	**cpx129_A**	**cpx118p1_D**	**cpx129_C**
SiO_2	48.55(24)	50.40(24)	**SiO_2**	48.61(24)	50.30(25)	47.23(23)	46.33(23)	51.24(24)	**SiO_2**	39.17(19)	43.76(22)	44.07(22)
TiO_2	0.10(3)	0.11(3)	**TiO_2**	0.95(4)	0.67(3)	1.21(5)	1.93(8)	0.87(4)	**TiO_2**	1.04(4)	1.40(5)	1.14(4)
Al_2O_3	32.26(19)	29.40(11)	**Al_2O_3**	14.07(12)	16.88(15)	10.54(9)	11.78(10)	12.63(12)	**Al_2O_3**	6.01(5)	8.63(8)	10.25(9)
FeO	0.71(7)	0.92(7)	**FeO**	6.71(17)	5.56(14)	8.46(21)	9.73(24)	6.07(16)	**FeO**	7.46(18)	8.30(20)	7.40(18)
MnO	-	0.03(4)	**MnO**	0.24(10)	0.06(3)	0.18(8)	0.26(11)	0.12(4)	**MnO**	0.25(10)	0.21(9)	0.25(11)
MgO	0.04(2)	0.04(2)	**MgO**	7.55(11)	6.43(10)	11.36(17)	9.51(14)	8.52(10)	**MgO**	9.24(14)	10.47(15)	9.49(14)
CaO	16.42(14)	13.56(12)	**CaO**	16.32(18)	14.82(16)	19.20(21)	16.48(18)	15.74(13)	**CaO**	25.69(28)	18.57(20)	21.52(24)
Na_2O	1.84(6)	3.18(8)	**Na_2O**	1.30(4)	1.52(5)	1.18(4)	1.41(4)	2.04(7)	**Na_2O**	0.82(3)	2.27(7)	1.06(3)
K_2O	0.44(3)	0.37(2)	**K_2O**	1.77(3)	2.88(5)	0.92(2)	1.54(3)	0.89(3)	**K_2O**	0.38(1)	0.49(1)	0.75(1)
P_2O_5	0.08(4)	0.05(4)	**P_2O_5**	0.47(5)	0.49(5)	0.04(0)	0.17(2)	1.07(9)	**P_2O_5**	8.26(82)	5.29(53)	3.88(38)
Total	100.44	98.06	**Total**	97.98	99.60	100.32	99.15	99.18	**Total**	98.32	99.39	99.80
Ab	16	29	**CaO/Na_2O**	13	10	16	12	8	**CaO/Na_2O**	31	8	20
An	81	69	**(CaO/Na_2O)corr**						**(CaO/Na_2O)cor**	13	3	5
Or	3	2	**Sc**	73(239)	56(323)	52(178)	65(267)		**Sc**	109(338)	96(268)	79(320)
Sc	-	-	**V**	326(14)	255(20)	323(10)	533(15)		**V**	465(22)	469(17)	409(21)
V	-	-	**Cr**	62(11)	63(16)	540(8)	109(13)		**Cr**	248(19)	325(12)	198(18)
Cr	-	-	**Ni**	62(7)	72(7)	73(5)	54(7)		**Ni**	76(11)	-	-
Ni	-	141(6)	**Rb**	69(40)	70(49)	90(32)	57(42)		**Rb**	-	12(44)	14(49)
Rb	-	-	**Sr**	726(4)	1005(5)	319(3)	464(4)		**Sr**	200(5)	163(4)	638(4)
Sr	1752(5)	1393(4)	**Y**	23.8(5.6)	15.4(5.7)	21.9(4.0)	28.7(4.1)		**Y**	51.4(5.7)	41.9(5.8)	59.9(5.4)
Y	-	-	**Zr**	99(2)	70(3)	83(2)	94(3)		**Zr**	131(3)	130(2)	116(3)
Zr	-	-	**Nb**	6.9(7.0)	5.7(10.2)	22.8(4.4)	37.6(6.9)		**Nb**	2.4(9.5)	4.9(8.0)	2.7(8.9)
Nb	-	-	**Ba**	778(3)	1542(3)	279(2)	499(3)		**Ba**	58(3)	138(2)	389(3)
Ba	439(3)	145(3)	**La**	19.9(2.2)	13.2(3.7)	10.4(3.4)	15.7(2.2)		**La**	55.6(4.5)	17.2(2.2)	74.1(4.3)
La	5.3(3.7)	7.5(4.4)	**Ce**	44.8(2.1)	31.2(3.0)	32.1(1.4)	43.4(2.0)		**Ce**	127.9(2.2)	52.8(1.7)	169.1(2.1)
Ce	7.6(2.9)	21.3(1.9)	**Nd**	34.8(2.6)	23.6(5.7)	20.4(3.2)	39.3(3.5)		**Nd**	98.6(5.9)	42.4(4.3)	105.0(5.5)
Nd	-	6.9(3.4)	**Sm**	7.5(2.7)	8.2(3.4)	10.2(1.6)	6.7(2.4)		**Sm**	20.1(4.0)	14.9(2.6)	23.6(3.8)
Sm	-	-	**Eu**	2.5(2.1)	1.6(3.2)	1.5(2.2)	1.8(2.8)		**Eu**	4.7(4.0)	3.2(3.0)	5.9(3.7)
Eu	-	-	**Yb**	1.7(1.3)	-	2.0(1.7)	3.6(2.0)		**Yb**	3.6(2.5)	2.7(1.4)	4.2(2.4)
Yb	-	-	**CO_2**	1717 ± 240	283 ± 40			362 ± 51	**CO_2**	179 ± 25		
			H_2O	0.15 ± 0.01	0.14 ± 0.01			0.04 ± 0.00	**H_2O**	0.12 ± 0.01		
			F	980 ± 49	482 ± 24			350 ± 17	**F**	768 ± 38		
			S	103 ± 6	47 ± 3			31 ± 2	**S**	41 ± 2		
			Cl	652 ± 156	513 ± 123			129 ± 31	**Cl**	350 ± 84		
			Tq	1256		1251	1256	1250	**Tq**	1241	1245	1241
			host mg#	0.82	0.83	0.85	0.85	0.82	**host mg#**	0.85	0.88	0.83

(continued)

Table 2. Composition of representative RMI in clinopyroxene (continued)

	Type I RMI												
Sample	**cpx165_B**	**cpx153_E**	**cpx151_D**	**cpx143_B**	**cpx143_C**	**cpx140_D**	**cpx110_B**	**cpx05_B**	**cpx117_A**	**cpx116_A**	**cpx159_A**	**cpx139_C**	**cpx150_A**
SiO_2	49.99(24)	52.31(24)	53.98(27)	50.14(26)	52.39(27)	52.32(27)	52.43(26)	51.57(26)	51.78(26)	48.74(24)	50.77(24)	52.50(27)	51.97(27)
TiO_2	1.29(5)	1.11(4)	0.93(4)	1.20(4)	1.04(4)	1.31(5)	0.98(4)	1.19(5)	1.39(5)	1.37(5)	1.34(5)	1.21(5)	1.32(5)
Al_2O3	11.80(11)	15.17(13)	15.66(13)	13.03(12)	15.43(13)	15.65(13)	11.99(11)	11.80(10)	16.14(14)	14.08(12)	14.70(13)	12.87(12)	15.39(13)
FeO	7.85(18)	6.91(17)	5.38(15)	7.02(17)	6.12(16)	7.37(18)	6.66(16)	8.39(21)	8.43(21)	12.27(30)	8.67(19)	7.05(17)	7.10(17)
MnO	0.11(5)	0.09(5)	0.08(4)	0.13(4)	0.10(5)	0.13(5)	0.21(9)	0.22(9)	0.18(7)	0.16(7)	0.14(4)	0.12(5)	0.09(4)
MgO	7.90(10)	4.21(7)	5.24(8)	8.04(10)	4.88(8)	4.56(8)	8.43(12)	8.35(12)	4.35(6)	5.39(8)	5.03(8)	7.09(9)	4.81(8)
CaO	13.30(12)	6.63(9)	8.03(10)	12.82(12)	8.43(10)	8.00(9)	13.10(14)	13.85(15)	8.49(9)	9.77(11)	8.32(10)	12.18(12)	7.22(9)
Na_2O	1.76(6)	3.02(8)	2.27(7)	1.85(6)	2.15(7)	2.77(8)	1.74(5)	1.53(5)	2.62(8)	2.65(8)	2.67(8)	2.13(7)	3.18(8)
K_2O	3.53(6)	6.65(9)	6.57(9)	4.21(7)	6.52(9)	6.09(8)	3.85(6)	3.47(6)	5.24(9)	4.14(7)	5.65(8)	4.00(7)	6.21(8)
P_2O_5	0.68(7)	0.72(7)	0.73(8)	0.66(7)	0.83(8)	0.98(8)	0.72(7)	0.37(4)	0.74(7)	0.72(7)	0.80(8)	0.57(7)	0.89(8)
Total	98.22	96.82	98.85	99.10	97.87	99.18	100.12	100.73	99.34	99.30	98.10	99.72	98.18
CaO/Na_2O	8	2	4	7	4	3	8	9	3	4	3	6	2
Sc	74(186)	-	-	-	-	-	53(208)	55(371)	45(215)	75(254)	-	70(151)	-
V	336(10)	262(24)	342(29)	332(13)	301(13)	302(18)	275(14)	371(21)	251(12)	371(15)	316(18)	322(9)	306(20)
Cr	224(9)	46(21)	547(26)	331(11)	140(11)	59(15)	130(11)	151(18)	25(12)	505(12)	57(15)	210(8)	67(15)
Ni	78(5)	-	-	-	84(5)	-	67(5)	-	62(7)	-	201(7)	59(4)	-
Rb	126(51)	232(112)	62(287)	180(117)	229(120)	167(180)	219(33)	135(59)	237(33)	72(46)	125(74)	168(84)	218(172)
Sr	405(2)	544(5)	289(6)	374(4)	576(4)	582(4)	510(3)	452(6)	544(3)	282(5)	388(5)	386(3)	500(4)
Y	27.1(3.2)	20.8(6.7)	28.7(7.7)	24.4(4.8)	18.0(4.9)	27.3(5.3)	22.8(3.5)	35.4(5.7)	23.7(3.5)	31.9(5.7)	41.5(5.9)	27.5(2.7)	20.0(4.5)
Zr	173(2)	188(4)	111(7)	187(3)	174(3)	238(4)	133(4)	161(4)	190(3)	144(2)	265(3)	174(1)	229(2)
Nb	25.0(5.4)	40.6(11.8)	11.1(16.6)	27.7(6.8)	38.5(7.0)	44.4(9.2)	18.9(5.8)	22.8(9.6)	37.2(5.8)	18.2(6.2)	27.4(7.7)	24.4(4.6)	40.6(9.1)
Ba	1292(2)	2076(5)	660(4)	1265(2)	2115(2)	2095(3)	1464(2)	1271(4)	1967(2)	822(3)	1246(4)	1356(2)	2052(3)
La	34.0(1.4)	45.3(6.1)	19.2(8.5)	32.8(3.0)	41.6(3.1)	52.1(3.3)	33.6(2.8)	41.2(3.1)	51.8(2.6)	25.1(4.8)	41.0(3.0)	35.3(2.4)	49.4(3.4)
Ce	74.6(1.0)	85.3(3.8)	46.1(5.1)	72.4(2.4)	74.4(2.4)	100.4(2.3)	71.2(1.7)	76.2(2.8)	97.6(1.6)	62.1(2.0)	85.3(2.6)	71.7(1.5)	89.2(3.9)
Nd	41.6(3.0)	40.0(5.8)	31.2(6.8)	37.8(3.5)	33.4(3.6)	45.5(4.9)	38.1(3.5)	37.2(4.8)	46.7(2.7)	43.5(4.5)	54.5(3.6)	38.3(2.8)	41.4(4.6)
Sm	8.8(1.8)	9.9(4.5)	-	7.2(2.9)	4.8(3.1)	7.7(3.6)	8.0(1.6)	14.2(3.3)	8.6(1.4)	10.1(2.3)	9.0(1.8)	9.0(1.8)	10.6(2.6)
Eu	2.5(1.7)	3.1(3.2)	-	2.2(2.8)	1.8(2.9)	2.6(3.3)	1.9(3.1)	2.5(3.9)	2.4(2.9)	2.6(3.1)	3.9(2.1)	2.2(2.0)	1.5(3.6)
Yb	2.2(1.4)	-	-	-	-	2.1(3.0)	1.7(1.3)	4.5(2.8)	1.8(1.8)	2.3(2.4)	-	2.4(0.9)	2.8(2.0)
CO_2	382 ± 53	295 ± 41	220 ± 31		266 ± 37	297 ± 42	220 ± 31	268 ± 38	497 ± 70	216 ± 30	645 ± 90		272 ± 38
H_2O	0.07 ± 0.00	0.04 ± 0.00	0.04 ± 0.00		0.05 ± 0.00	0.05 ± 0.00	0.08 ± 0.00	0.12 ± 0.01	0.19 ± 0.01	0.14 ± 0.01	0.08 ± 0.00		0.04 ± 0.00
F	1951 ± 98		1364 ± 68					2211 ± 111	914 ± 46	4262 ± 213	1812 ± 91		
S	70 ± 4	100 ± 6	49 ± 3		77 ± 5	106 ± 6	155 ± 9	132 ± 8	150 ± 9	129 ± 8	111 ± 7		101 ± 6
Cl	647 ± 155	686 ± 165	547 ± 131		872 ± 209	912 ± 219	2546 ± 611	1185 ± 284	2226 ± 534	1710 ± 410	903 ± 217		843 ± 202
Tq	1229	1225	1224	1241	1241	1233	1255	1256	1240	1251	1224	1243	1213
host mg#	0.82	0.83	0.82	0.80	0.82	0.77	0.86	0.88	0.81	0.83	0.79	0.78	0.78

mg# = Mg/(Mg+Fe^{2+}); Ab,An, Or, albite, anorthite and orthoclase in mol% of feldspar; -, below detection limit; (CaO/Na_2O)corr, CaO/Na_2O ratio after subtracting apatite; Tq, quenching temperature;host mg#, mg# of the host clinopyroxene; major and minor elements and H2O are in wt%, all others in ppm. Major and minor elements were determined by EPMA, trace elements by LA-ICP-MS, volatile elements by SIMS. Estimated standard deviation (e.s.d.) is indicated in parentheses. In case of SIMS analyses, the estimate of the measurement error is shown.

Table 3. Predicted formation conditions of clinopyroxene calculated by different geothermobarometers

<table>
<tr><th></th><th>Putirka et al. (1996)</th><th>Putirka et al. (2003)</th><th>Putirka (2008)</th></tr>
<tr><td><i>T</i></td><td>1043-1246 °C ± 27 °C</td><td>980-1309 °C ± 33 °C</td><td>1019-1366 °C ± 58 °C</td></tr>
<tr><td>$T_{average}$</td><td>1186 °C ± 15 °C</td><td>1152 °C ± 33 °C</td><td>1184 °C ± 58 °C</td></tr>
<tr><td>Pressure</td><td>120-1630 MPa ± 100 MPa</td><td>-280-1160 MPa ± 170 Mpa</td><td>160-2480 kMPa ± 310 Mpa</td></tr>
<tr><td></td><td>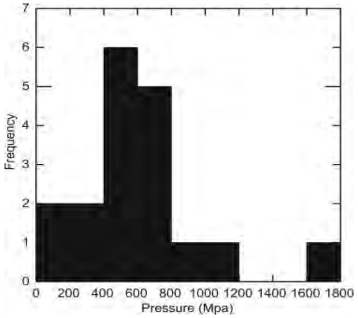
</td><td>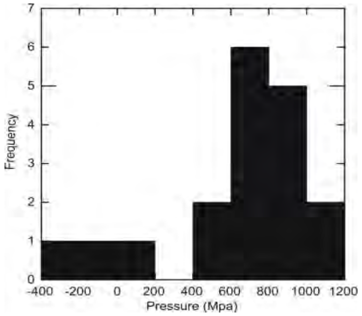
</td><td>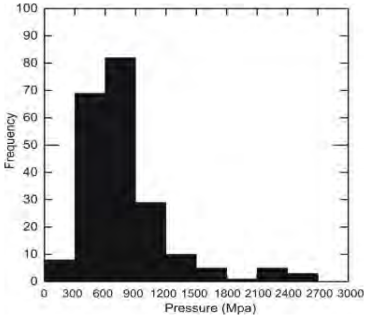
</td></tr>
</table>

Figure 1.

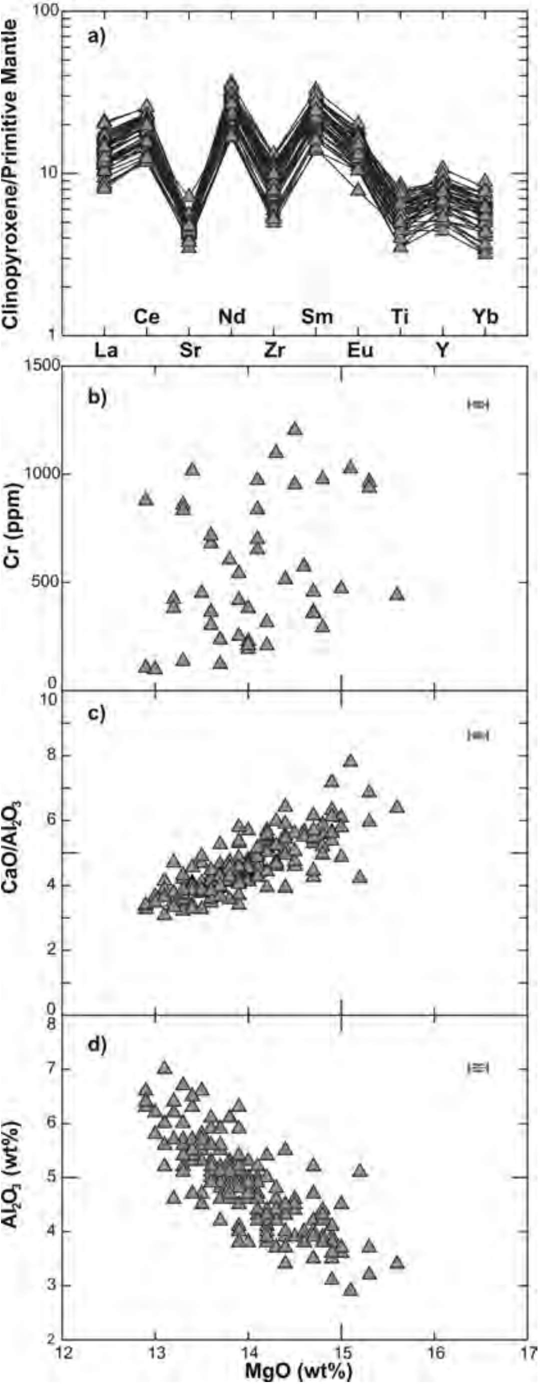

a)
Clinopyroxene/Primitive Mantle
100
10
1
La
Ce
Sr
Nd
Zr
Sm
Eu
Ti
Y
Yb
b)
Cr (ppm)
1500
1000
500
0
c)
CaO/Al$_2$O$_3$
10
8
6
4
2
0
d)
Al$_2$O$_3$ (wt%)
8
7
6
5
4
3
2
12
13
14
15
16
17
MgO (wt%)

Figure 2.

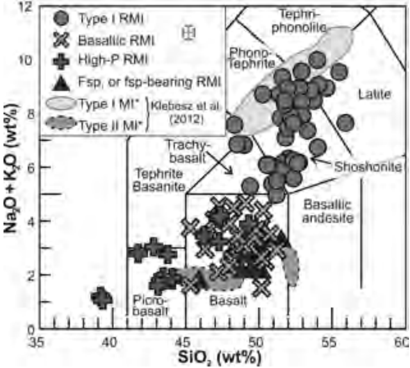

Type I RMI
Basaltic RMI
High-P RMI
Fsp, or fsp-bearing RMI
Type I MI*
Type II MI*
Klebesz et al. (2012)
Tephri-phonolite
Phono-Tephrite
Latite
Trachy-basalt
Shoshonite
Tephrite Basanite
Basaltic andesite
Picro-basalt
Basalt
$Na_2O + K_2O$ (wt%)
SiO_2 (wt%)
0
2
4
6
8
10
12
35
40
45
50
55
60

Figure 3.

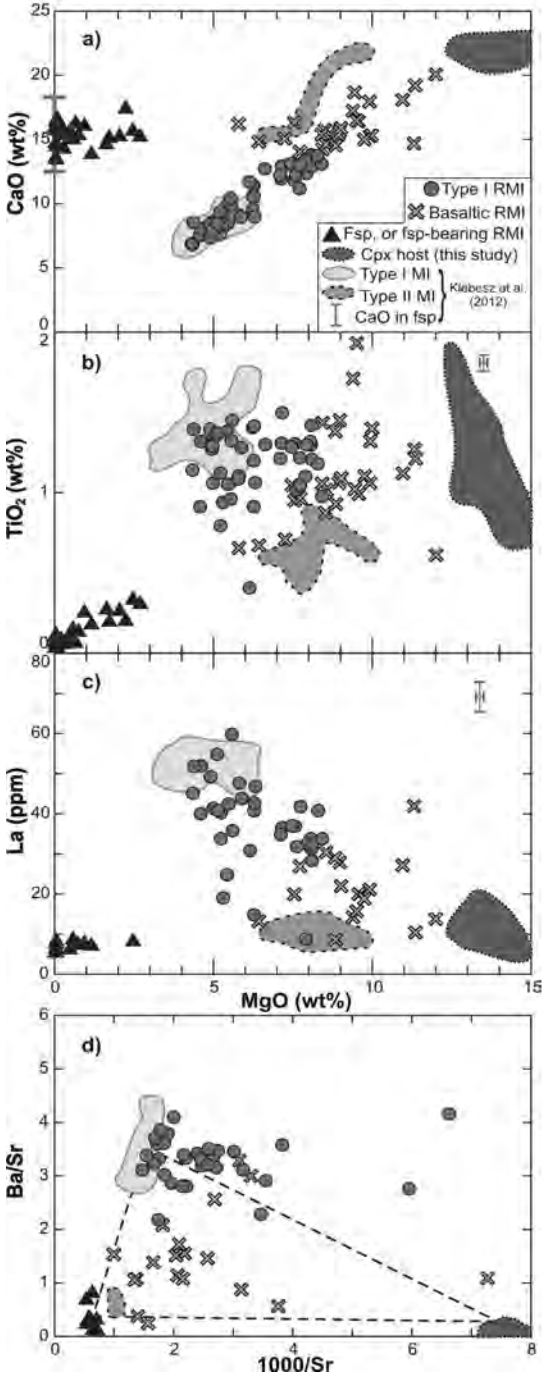
a)
CaO (wt%)
25
20
15
10
5
0
Type I RMI
Basaltic RMI
Fsp, or fsp-bearing RMI
Cpx host (this study)
Type I MI
Type II MI
Klebesz et al. (2012)
CaO in fsp
b)
TiO₂ (wt%)
2
1
0
c)
La (ppm)
80
60
40
20
0
MgO (wt%)
0
5
10
15
d)
Ba/Sr
6
5
4
3
2
1
0
1000/Sr
0
2
4
6
8

Figure 4.

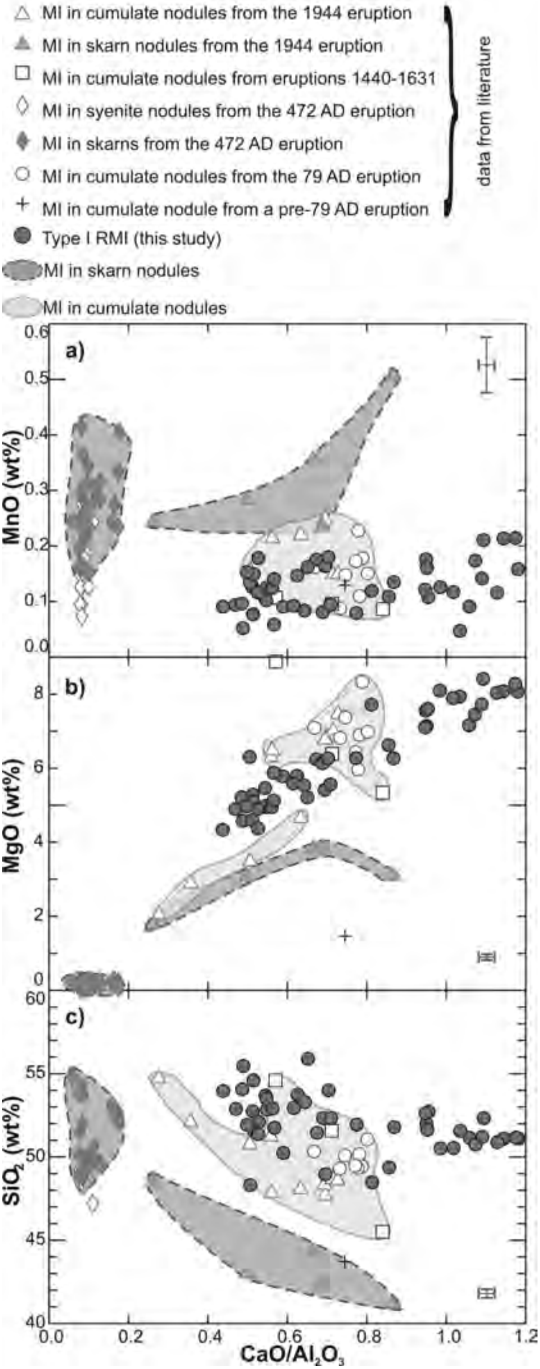
△ MI in cumulate nodules from the 1944 eruption
▲ MI in skarn nodules from the 1944 eruption
□ MI in cumulate nodules from eruptions 1440-1631
◇ MI in syenite nodules from the 472 AD eruption
◆ MI in skarns from the 472 AD eruption
○ MI in cumulate nodules from the 79 AD eruption
+ MI in cumulate nodule from a pre-79 AD eruption
data from literature
● Type I RMI (this study)
MI in skarn nodules
MI in cumulate nodules
a)
MnO (wt%)
0.6
0.5
0.4
0.3
0.2
0.1
0.0
b)
MgO (wt%)
8
6
4
2
0
c)
SiO$_2$ (wt%)
60
55
50
45
40
0.0
0.2
0.4
0.6
0.8
1.0
1.2
CaO/Al$_2$O$_3$

Figure 5.

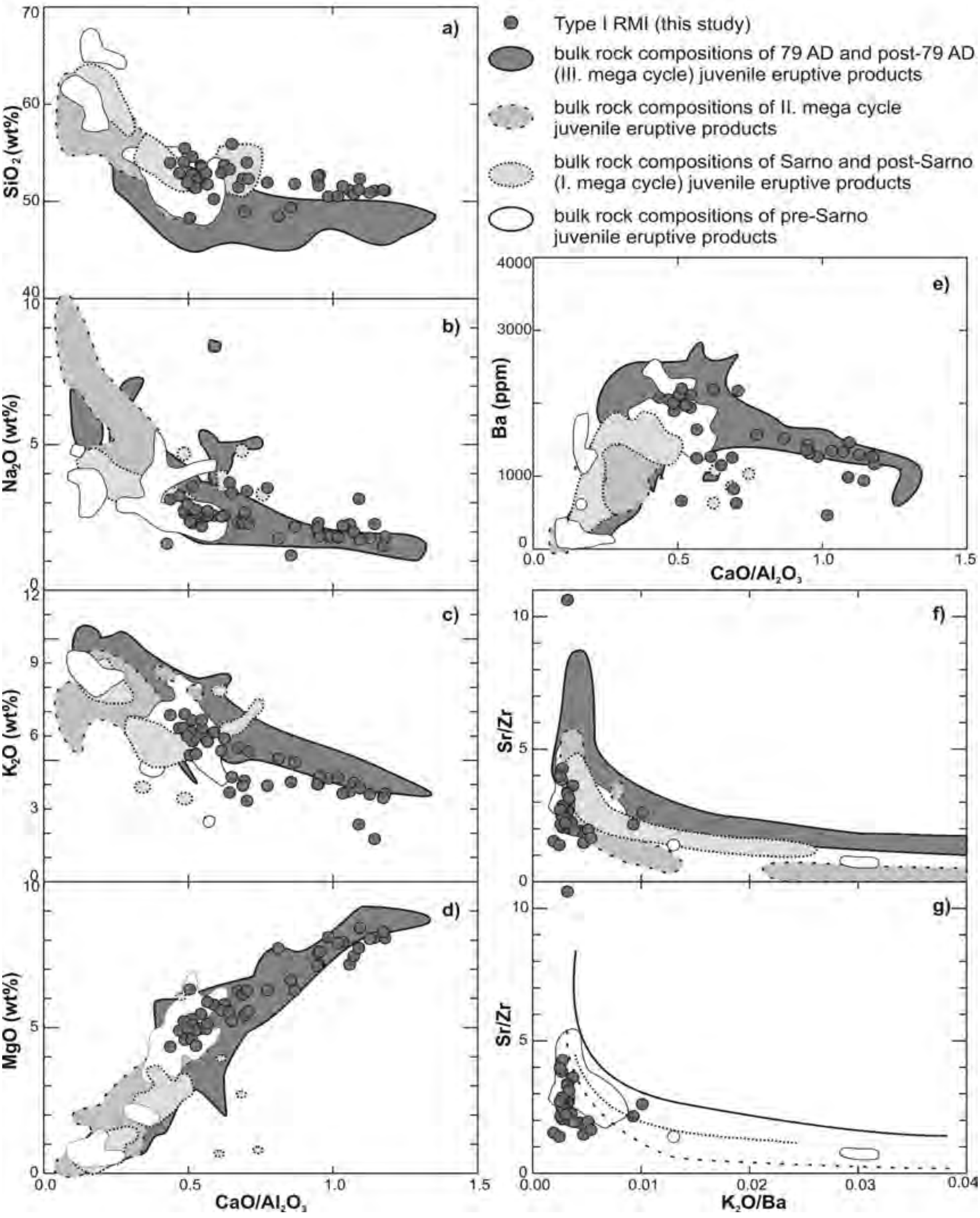
a)
b)
c)
d)
e)
f)
g)
SiO₂ (wt%)
Na₂O (wt%)
K₂O (wt%)
MgO (wt%)
CaO/Al₂O₃
Ba (ppm)
Sr/Zr
K₂O/Ba
70
60
50
40
10
5
0
12
9
6
3
4000
3000
1000
0.0
0.5
1.0
1.5
0.00
0.01
0.02
0.03
0.04
Type I RMI (this study)
bulk rock compositions of 79 AD and post-79 AD (III. mega cycle) juvenile eruptive products
bulk rock compositions of II. mega cycle juvenile eruptive products
bulk rock compositions of Sarno and post-Sarno (I. mega cycle) juvenile eruptive products
bulk rock compositions of pre-Sarno juvenile eruptive products

Figure 6.

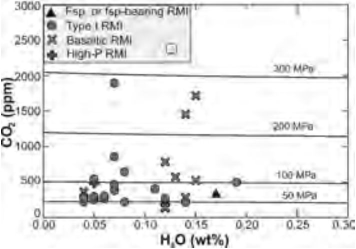

▲ Fsp. or fsp-bearing RMI
● Type I RMI
✖ Basaltic RMI
✚ High-P RMI
300 MPa
200 MPa
100 MPa
50 MPa
CO_2 (ppm)
0
500
1000
1500
2000
2500
3000
H_2O (wt%)
0.00
0.05
0.10
0.15
0.20
0.25
0.30